N-63-4-3

FORWARDED BY THE CHIEF, BUREAU OF SHIPS 210L

THEORETICAL QUARTERLY PROGRESS REPORT

NO. 4

THIS DOCUMENT MAY BE RELEASED WITH NO RESTRICTIONS ON DISSEMINATION

Westinghouse Research Laboratories
Pittsburgh 35, Pennsylvania

THEORETICAL QUARTERLY PROGRESS REPORT

NO. 4
FINAL REPORT

U.S. Navy - BuShips
Contract No. NOBS-84687
W. G. O. No. WG 80389 CE

TABLE OF CONTENTS

Summary

Bismuth telluride and its alloys are the most important thermoelectric materials for applications near room temperature. In the past, it has always been made n-type by adding a foreign impurity. In the first section of this report, some measurements are reported on material made n-type by adding excess tellurium. At very low temperatures, the electron mobility is about ten times larger than has been previously reported. In the temperature range where the material is a useful thermoelectric material, there is little change in the mobility. However, the larger mobility at helium temperatures may allow one to do experiments such as cyclotron resonance which will give a better measurement of the electronic band structure than has been possible previously.

The second paper gives the results of an investigation of the Seebeck coefficient, thermal conductivity, and electrical conductivity of bismuth single crystals. Bismuth-antimony alloys have been used as thermoelectric device elements for many years, and they have the highest figure of merit of any material at temperatures near 100°K. In this work, some of the properties of the band structure and the lattice thermal conductivity have been determined. The optimum figure of merit of the material has been calculated.

Scientific Paper 62-129-104-P4 June 11, 1962

HIGH MOBILITY N-TYPE BISMUTH TELLURIDE

Roland W. Ure, Jr.

Westinghouse Research Laboratories
Beulah Road, Churchill Borough
Pittsburgh 35, Pennsylvania

Scientific Paper 62-129-104-P4 June 11, 1962

HIGH MOBILITY N-TYPE BISMUTH TELLURIDE

Roland W. Ure, Jr.
Westinghouse Research Laboratories
Pittsburgh 35, Pa., U.S.A.

ABSTRACT

Samples of n-type bismuth telluride with carrier concentrations between 3×10^{17} and 6×10^{19} cm^{-3} have been made by doping with excess tellurium. The largest mobility at 4.2°K is 1.8×10^{5} $cm^2/Vsec$, approximately ten times larger than has been observed in n-type iodine doped bismuth telluride. At a carrier concentration of about 5×10^{18} cm^3, there is a sharp change in slope of the curve of 4.2°K mobility *vs* carrier concentration. These results are interpreted on the basis of a two-band model. Seebeck coefficient measurements tend to confirm this model.

I. INTRODUCTION

The compound Bi_2Te_3 is an anisotropic semiconductor with a rhombohedral structure and a very pronounced cleavage. When grown from a stoichiometric melt, it is p-type with a carrier concentration of the order of 10^{19} holes/cm^3. The reason for this high carrier concentration is that the maximum melting composition is on the bismuth rich side of the

stoichiometric composition (Offergeld and Van Cakenberghe, 1959) and hence a crystal grown from a stoichiometric melt contains excess Bi. This excess Bi acts as an acceptor in the crystal. Measurements of a number of different properties of both n and p-type material have been made (for review of the properties of Bi_2Te_3, see Ure, 1961) but the carrier concentration is usually changed by adding a foreign impurity such as iodine. We have reported earlier some data on n and p-type material in which the carrier concentration was altered by changing the Bi:Te ratio in the crystal (Satterthwaite and Ure, 1957). Sladek (1959) has measured one of our samples and found a $4.2^{\circ}K$ mobility approximately ten times larger than has been reported elsewhere.

In this paper, we report measurements of Hall coefficient and mobility over a wider range of temperature ($4.2^{\circ}K$ to $250^{\circ}K$) and carrier concentration (3×10^{17} to 6×10^{19}) for n-type samples. We find mobilities as high as 180,000 $cm^2/Vsec$ at $4.2^{\circ}K$. At room temperature, the mobility is about the same as for iodine doped samples.

II. EXPERIMENTAL

All samples measured were single crystals and were grown from melts containing from 63 to 67 atomic percent tellurium. Both Bridgman and zone leveling techniques were used. Considerable difficulty was experienced in obtaining reasonably homogeneous samples, particularly at carrier concentrations below 10^{18} cm^{-3}. In samples grown by the Bridgman procedure, there is a regular increase in the carrier concentration from the bottom to the top of the crystal because of the increase in Te content of the liquid as the crystal freezes. However, some uniform samples were obtained by cutting samples perpendicular to the growth direction.

Samples were cut with a spark cutter (Chandrasekhar, 1961; Cole, Bucklow, and Bridgeon, 1961). The edges of the samples which were damaged during the cutting operation were cleaved off and the samples were etched in 1:1 HCl:H_2O_2 to clean the surfaces and to detect cracks in the samples. Crack-free samples were usually obtained by this procedure. Sample dimensions varied from about 1 x 1 x 10 mm to 2 x 3 x 20 mm.

The ends of the samples were nickel plated and platinum current leads were soldered to the plating. Platinum-rhodium pressure contacts were used for potential probes. Four probes were placed on the samples -- two on each side -- so that two resistivity and two Hall measurements could be made. On the better samples (indicated by filled points on the curves) the two Hall measurements differed by less than 15% and the two resistivity measurements differed by less than 10%. All measurements were made by standard dc potentiometric methods. In measuring resistivities, the readings were first made with the current flowing in one direction. Then a reading was taken immediately after reversing the current before the temperature distribution in the sample changed. In this way, thermal emf's resulting from the temperature inhomogeneity produced by the Peltier effect were eliminated. Hall effect measurements were made in a field of 6 kG. Readings were taken with both current and field in the forward and reverse directions, and the appropriate average of four readings was used. All measurements were made with the magnetic field perpendicular to the

cleavage planes and the current in the cleavage plane. Temperatures were measured with a carbon resistor or with a copper-constantan thermocouple both calibrated against a standard platinum resistor.

The measured Hall coefficients are shown in Fig. 1. Carrier concentrations, n, were calculated from the equation

$$n = Br/Re \qquad (1)$$

using the average of the two Hall measurements R at 77°K. Here B is a factor depending on the band structure and is unity for spherical bands. From magnetoresistance measurements on iodine doped samples, Drabble, Groves, and Wolfe (1958) showed that the Bi_2Te_3 has a multivalley conduction band with highly oblate constant energy surfaces. They found B = 0.326. However, Goldsmid (1961) and Walker (1960) have found that this factor is a function of the carrier concentration in the specimen. Because of the significant differences between the properties of iodine doped and tellurium doped samples reported here, the factor may be different in our samples. Because of these uncertainties, we have not corrected our data, but have taken B = 1. The factor r depends on the scattering mechanism and the degree of degeneracy. We have taken r = 1 since the scattering mechanisms have not been established. Hall mobilities μ were calculated from $\mu = R_{77}/\rho$. Values of the Hall mobility are shown in Fig. 2 and 3 and the resistivity ρ in Fig. 4. It must be

remembered that the "carrier concentration" quoted may be 3 times larger than the true carrier concentration and that the Hall mobility may be one-third of the conductivity mobility.

III. DISCUSSION

A. Hall Coefficient

The Hall coefficient, shown in Fig. 1, shows some variation with temperature in the extrinsic region. With increasing temperature, the Hall coefficient first falls slightly, goes through a shallow minimum near the temperature of liquid nitrogen, and then goes through a slight maximum before it falls rapidly as the samples become intrinsic. Yates (1959) observed a similar behavior in iodine doped bismuth telluride. In a semiconductor which has significant carrier densities in each of two different conduction bands with extrema at different energies and with different mobilities, the Hall coefficient vs temperature shows a maximum. Thus the observed maximum is evidence for the two band picture to be discussed later. The fact that sample D-13 with the lowest carrier concentration does not show this maximum may be evidence that the energy separation between the two bands is large enough that there are very few carriers in the upper band in this sample. However, this sample was fairly inhomogeneous.

B. Hall Mobility

The largest Hall mobility observed is 1.8×10^5 $cm^2/Vsec$ in sample B-2A with a "carrier concentration" of 9×10^{17} cm^3. This sample was reasonably uniform. The two Hall coefficients differed by 7 percent and the two resistivity measurements by one percent. This Hall mobility is ten times larger than the largest mobility observed by Yates (1959) on iodine doped samples.

In the region between 77°K and 200°K, the mobility varies as T^{-a} where a is a constant. The values for a are given in Table 1. Drabble, Groves, and Wolfe (1958), Goldsmid (1958), and Mansfield and Williams (1958) have all found values very close to $T^{-1.70}$ for iodine doped material.

The most obvious explanation for these differences is that iodine doped samples still have an appreciable density of excess bismuth acceptors and hence are heavily compensated. Thus in an iodine doped sample with a carrier concentration of 10^{18} cm^{-3}, there may be of the order of 10^{19} ionized bismuth acceptors plus 1.1×10^{19} ionized iodine donors. Thus the density of ionized impurity centers is of the order of 20 times as large as the carrier concentration. This ratio of the density of ionized impurities to the carrier concentration will decrease as the carrier concentration is increased by adding additional iodine. In the tellurium doped samples this ratio is one. Thus we expect that the difference between the mobility in iodine and tellurium doped samples will be largest for low carrier concentrations and will decrease as the carrier concentration increases. As shown on Fig. 3 this is indeed the case.

Since ionized impurity scattering becomes less important with increasing temperature, the difference in the temperature variation of the mobility in iodine and tellurium doped samples can be explained by assuming that there is still a small amount of ionized impurity scattering at 100°K in the compensated iodine doped samples. This idea is supported by the fact that the mobility at 77°K for iodine doped samples is 25 to 35 percent smaller than in our tellurium doped samples. [Data on R_H and resistivity at 77°K in iodine doped samples taken from Drabble, Grover, and Wolfe (1958) and Bowley, Delves, and Goldsmid (1958)]. However, Bowley, Delves, and Goldsmid (1958) have determined the value of s in the expression for the relaxation time $\tau = \tau_o E^s$ from measurements of the magneto-Seebeck effect, and they find a value close to the theoretical value for acoustic mode lattice scattering. The difference between their measured value and the theoretical value indicates that, although the amount of ionized impurity scattering is small, the amount of ionized impurity scattering increases with decreasing carrier concentration. Austin's (1960) free carrier absorption data indicate some ionized impurity scattering at 77°K in iodine doped samples.

C. Magnitude of Mobility at 4.2°K

In the degenerate case, the mobility due to ionized impurity scattering (Brooks, 1955; Dingle, 1955; and Mansfield, 1956) is

$$\mu_I = 3\epsilon_o^2 h^3 n/16\pi^2 m_m m_d e^3 N_I f(b), \qquad (2)$$

where

$$f(b) = \ln(1+b)-b(1+b)^{-1},$$
$$b = (3n/\pi)^{1/3}(\epsilon_o h^2/4m_d e^2),$$

ϵ_o is the static dielectric constant, n is the carrier concentration, m_m is the mobility effective mass, m_d is the density-of-states effective mass, and N_I is the concentration of scattering impurities. Brooks (1955) has discussed the relation between the mobility mass and the mass tensor for the individual valleys. For the purposes of our estimates we will take $m_m = m_d$. Austin (1958) has measured an optical dielectric constant of 85. Since the static dielectric constant will be larger than this, we will assume a value of 100. In order to have a mobility of 1.8×10^5 $cm^2/Vsec$ with 10^{18} carriers an effective mass of 0.055 m_o must be used. In Table II we have shown values of the effective mass derived from Walker's data (1960) on iodine doped material and our measurements on one sample shown in Fig. 5. Here we have used the standard theory for the Seebeck coefficient assuming that the relaxation time is of the form $\tau = \tau_o E^s$. Values are given for s = 1/2, the value for acoustic mode lattice scattering, and s = 3/2, the simple theory for ionized impurity scattering. The values for other scattering mechanisms lie between these two. Since the predominant scattering mechanism in our sample at 100°K is probably acoustic mode lattice with small amounts of optic mode scattering, a reasonable estimate of the density-of-states mass is 0.2 m_o.

With this mass, a dielectric constant of 360 must be assumed in order to get agreement between Eq. 2 and our experimental values. In calculating the effective masses given in Table II, the constant B in Eq. 1 was taken as 1. If the value of B found by Drabble, Groves, and Wolfe (1958) were used, the effective masses shown in Table II would be multiplied by 0.47. However, to be consistent, we have to fit a mobility of 5.9×10^5 instead of 1.8×10^5, and the dielectric constant required is still 300. Thus there seems to be three possibilities: (1) Bismuth telluride has a static dielectric constant which is much larger than its optical dielectric constant, (2) the present theory of ionized impurity mobility is not accurate, or (3) our estimates of the effective mass are too large. A similar situation has been observed in lead telluride (Allgaier and Scanlon, 1958). From measurements of the polaron minimum in tunneling experiments on lead telluride, Hall (1960) has concluded that the static dielectric constant is not much larger than the optical dielectric constant in this material.

A number of objections to the present theory of ionized impurity scattering have been expressed (Herring, 1960). However, in our case the Born approximation should be valid since the dielectric constant is 100 or larger.

D. Variation of $4.2^{\circ}K$ Mobility with Carrier Concentration

As shown on Fig. 3, the mobility at $4.2^{\circ}K$ varies with carrier concentration as $n^{-0.28}$ for "carrier concentrations" less than 5×10^{18}

and as $n^{-1.20}$ for higher "carrier concentrations." The slope at the lower carrier concentration agrees with the theory of Eq. 2 within the experimental scatter of the data.

A rapid decrease in mobility with carrier concentration, similar to our data for $n > 5 \times 10^{18}$, has been found in PbTe (Kanai, Nii, and Watanabe, 1961). It has been explained by assuming that the scattering cross section remains independent of carrier concentration. The theory of ionized impurity scattering shows a rapid dependence of the relaxation time on the carrier velocity and thus a rapid variation of scattering cross section with carrier concentration in degenerate materials. Vinogradova, et al. (1959) have found that the scattering cross section for ionized impurities in a 80% Bi_2Te_3-20% Bi_2Se_3 alloy at temperatures of 100 to 300°K is independent of electron energy. They explain this by assuming that the large dielectric constant screens the Coulomb field sufficiently so that the major scattering is from the core of the impurity rather than from the Coulomb field of the impurity. This cannot be the explanation for our results at 4.2°K since the theoretical scattering by the screened Coulomb field alone gives a mobility smaller than that observed experimentally.

We are tempted to explain the change in slope of the curve of Fig. 3 as a two band effect. For carrier concentrations less than about 5×10^{18} cm^{-3}, all of the electrons are in one band. At higher concentrations, the electrons begin to fill a second band having a higher

effective mass and lower mobility. As donors are added and the total carrier concentration increases, the density of scattering centers N_I becomes larger than the carrier concentration in the lower band n_1, and the mobility of the electrons in the lower band decreases. Also since the upper band is assumed to have a larger mass, the electrons in the upper band will have a lower mobility than those in the lower band. Thus the average mobility will decrease with increasing carrier concentration. Preliminary calculations taking into account the proper relation between the Hall coefficient and the carrier concentration in each band seem to show that the rate of reduction in mobility should be smaller than observed experimentally. However, additional calculations are in progress. Yates (1959) and Walker (1960) have suggested that a two band model would explain some of the features of their work. The fact that the effective masses shown in Table II for more heavily doped material are appreciably larger than the masses calculated for our lightly doped sample D-13 is also evidence for this model.

Austin and Sheard (1957) have measured the optical energy gap of Bi_2Te_3 - Bi_2Se_3 alloys and find a sharp break in their curve at $Bi_2Te_{2.1}Se_{0.9}$. If we extrapolate the curve back to pure Bi_2Te_3 and assume that this energy difference of about 0.2 eV is the energy difference between the two conduction bands, we find that the lower band has a density-or-states of $0.05m_o$. This is just the value required to explain the large mobility.

IV. ACKNOWLEDGMENTS

We wish to thank G. R. Wagner for carefully performing most of the measurements reported here, D.A.Zupon for assistance with crystal growing, R. C. Miller and A. Sagar for several stimulating discussions, J. McHugh for growing some of the crystals, and C. B. Satterthwaite for the Seebeck coefficient data.

REFERENCES

Allgaier, R. S., and Scanlon, W. W., 1958, Phys. Rev. 111, 1029.

Austin, I. G., 1958, Proc. Phys. Soc. 72, 545.

Austin, I. G., 1960, Proc. Phys. Soc. 76, 169.

Austin, I. G., and Sheard, A., 1957, J. Electronics and Control 3, 2146.

Bowley, A. E., Delves, R., and Goldsmid, H. J., 1958, Proc. Phys. Soc. 72, 401.

Brooks, H., 1955, Advances in Electronics and Electron Physics, edited by L. Marton (New York: Academic Press).

Chandrasekhar, B. S., 1961, Rev. Sci. Instr. 32, 368.

Cole, M., Bucklow, I. A., and Grigson, C. W. B., 1961, Brit. J. Appl. Phys. 12, 296.

Dingle, R. B., 1955, Phil. Mag. 46, 831.

Drabble, J. R., Groves, R. D., and Wolfe, R., 1958, Proc. Phys. Soc. 71, 430.

Goldsmid, H. J., 1958, Proc. Phys. Soc. 71, 633.

Goldsmid, H. J., 1961, J. Appl. Phys. 32, 2198.

REFERENCES (continued)

Hall, E. N., 1960, Proceedings of the International Conference on Semiconductor Physics (Prague: Czechoslovak Academy of Sciences).

Herring, C., 1960, Proceedings of the International Conference on Semiconductor Physics (Prague: Czechoslovak Academy of Science), p. 63.

Kanai, Y., Nii, R., and Watanabe, N., 1961, J. Appl. Phys. 32, 2146.

Mansfield, R., and Williams, W., 1958, Proc. Phys. Soc. 72, 733.

Offergeld, G., and Van Cakenberghe, J., 1959, J. Phys. Chem. Solids 11, 310.

Satterthwaite, C. B. and Ure, R. W., Jr., 1957, Phys. Rev. 108, 1164.

Sladek, R. J., 1959, private communication; reported by Ure, 1961.

Ure, R. W., Jr., 1961, Thermoelectricity: Science and Engineering, edited by R. R. Heikes and R. W. Ure (Interscience Publishers, New York, 1961),p. 413.

Vinogradova, M. N., Golikova, O. A., Efimova, B. A., Kutasov, V. A., Stavitskaya, T. S., Stil'bans, L. S., and Sysoeva, L. M., 1959, Fiz. Tverdogo Tela 1, 1333 [English translation: Soviet Phys.-Solid State 1, 1224 (1960)].

Walker, P. A., 1960, Proc. Phys. Soc. 76, 113.

Yates, B., 1959, J. Electronics and Control, 6, 26.

Table I

Temperature Dependence of Mobility in

N-Type Tellurium Doped Bismuth Telluride

Sample	Carrier Concentration (cm^{-3})	Temperature Dependence of Mobility
D-13	2.4×10^{17}	$T^{-2.8}$
M3-1	5.3	$T^{-2.7}$
E1-2	3.0×10^{18}	$T^{-2.2}$
A2-1	3.4	$T^{-2.4}$
A4-1-5	1.2×10^{19}	$T^{-1.70}$
IU-1	6.8	$T^{-1.31}$

Table II

Values for Density-of-States Effective Mass Derived

from Seebeck Coefficient Data at 100°K

Sample Number	D-13	27	16	15	10
Source of Data	This paper	----------	Walker (1960)	---------	
"Carrier Concentration"	2.4×10^{17}	1.6×10^{18}	6×10^{18}	1.6×10^{19}	4×10^{19}
m_d/m_o for s = -1/2	0.26	0.64	0.67	0.96	1.00
m_d/m_o for s = 3/2	.07	0.21	0.21	0.31	0.34

FIGURE CAPTIONS

Fig. 1 Hall coefficient for tellurium doped n-type bismuth telluride. The symbols are identified on Fig. 2. The Hall coefficient is measured with the current in the cleavage plane and the magnetic field perpendicular to the cleavage plane.

Fig. 2 Electron Hall mobility in tellurium doped n-type bismuth telluride. Samples designated by solid symbols are more homogeneous, i.e., the two Hall coefficients differed by less than 15% and the two resistivities differed by less than 10%.

Fig. 3 Electron Hall mobility vs "electron concentration" at $4.2^{\circ}K$ and $77^{\circ}K$. Yates (1959) measurements at $4.2^{\circ}K$ on iodine doped samples are designated by a cross. All other points are our measurements on tellurium doped samples. Samples designated by solid symbols are more homogeneous than those designated by open or partially open symbols.

Fig. 4 Electrical resistivity for tellurium doped n-type bismuth telluride. The symbols are identified on Fig. 2.

Fig. 5 Seebeck coefficient for n-type tellurium doped and p-type zone refined bismuth telluride.

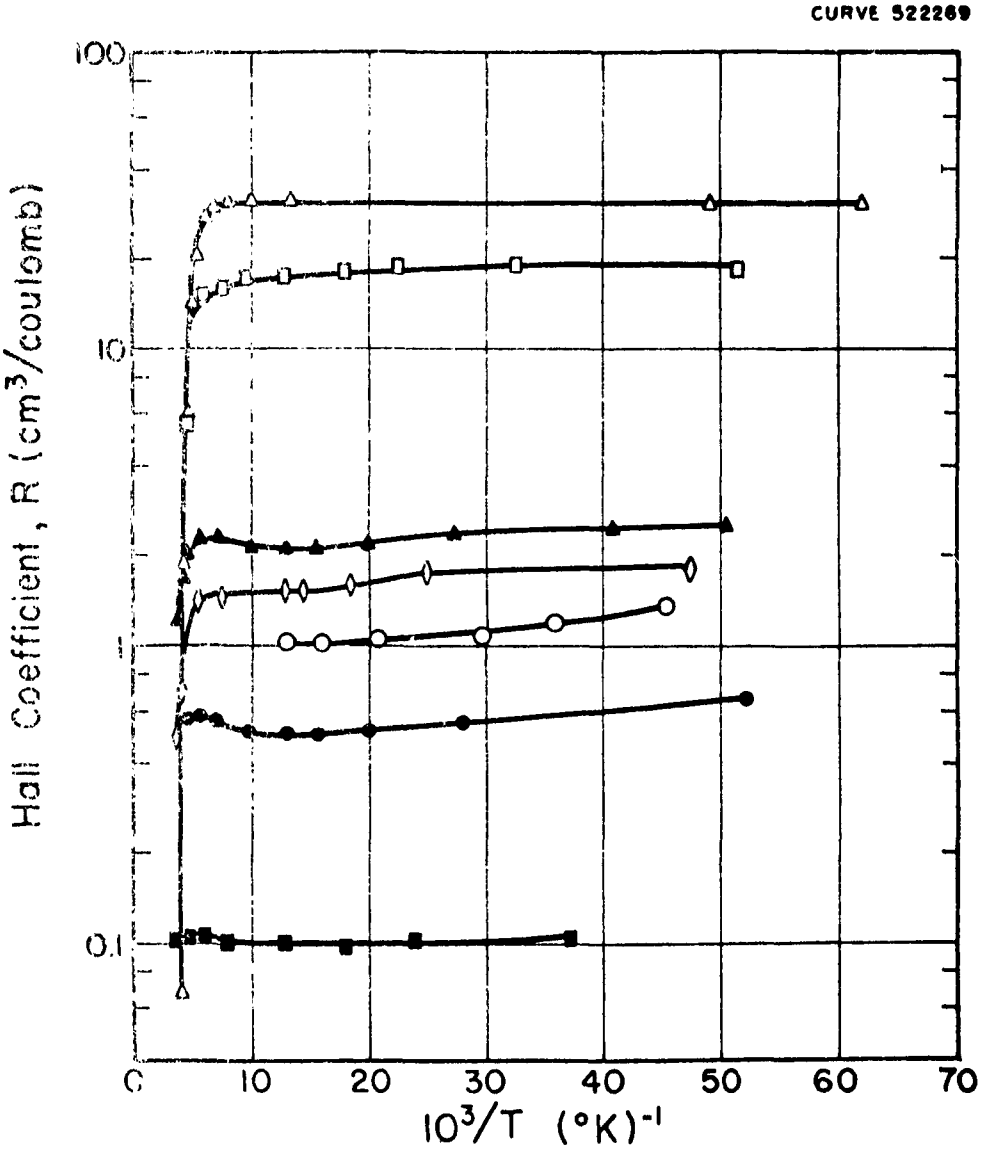

Fig.1- Hall coefficient for Te doped Bi_2Te_3

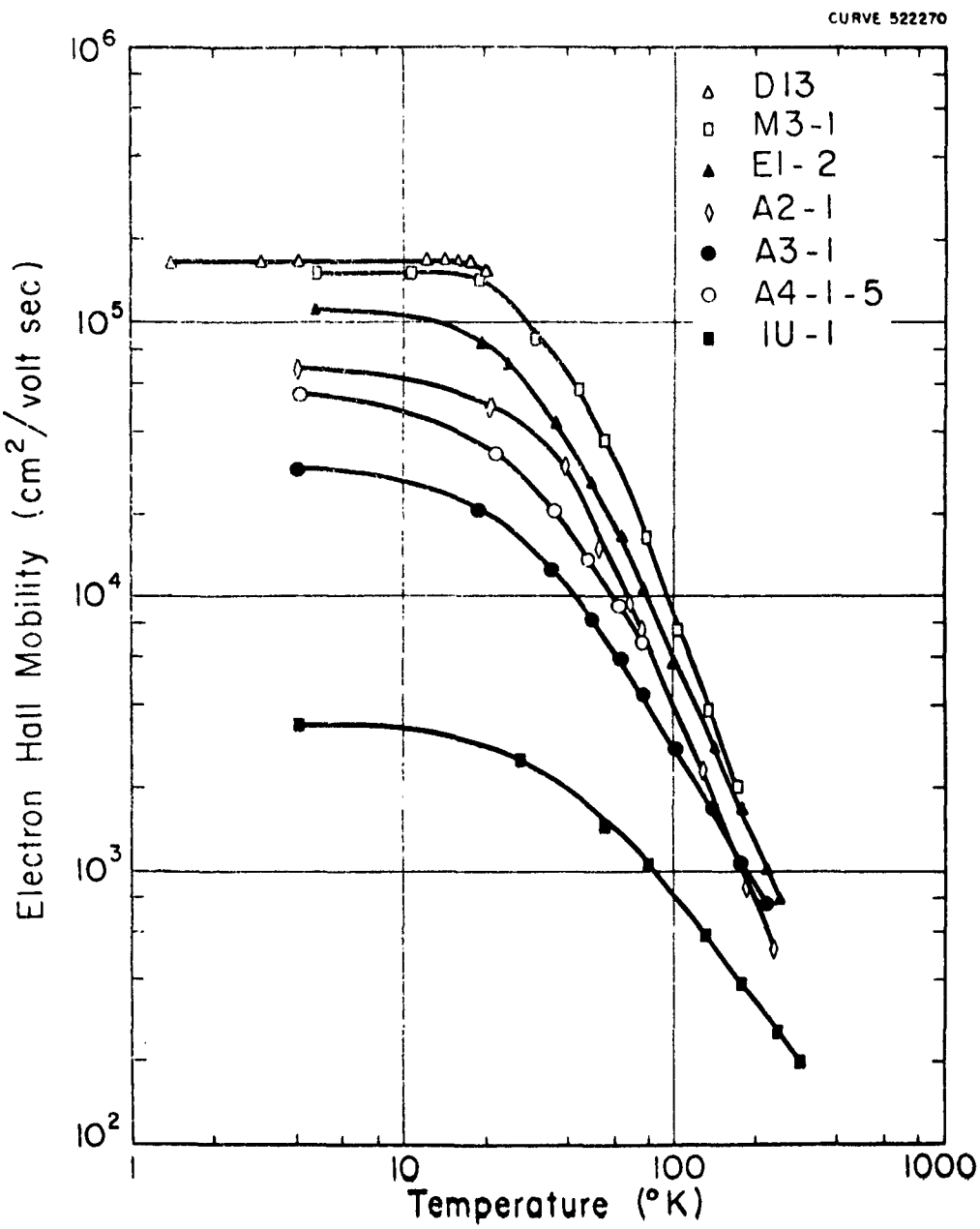

Fig. 2 - Electron Hall mobility for Te doped Bi_2Te_3

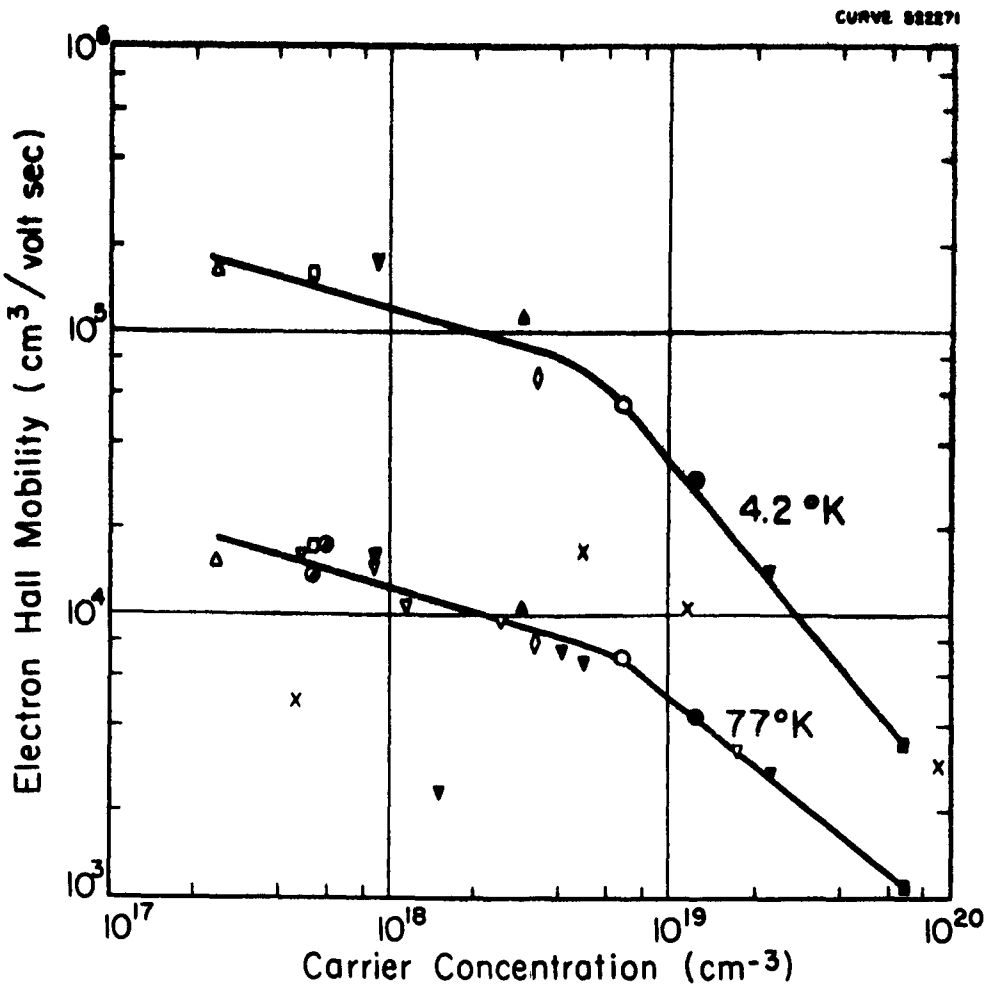

Fig. 3 - Hall mobility vs electron concentration for Te doped Bi_2Te_3

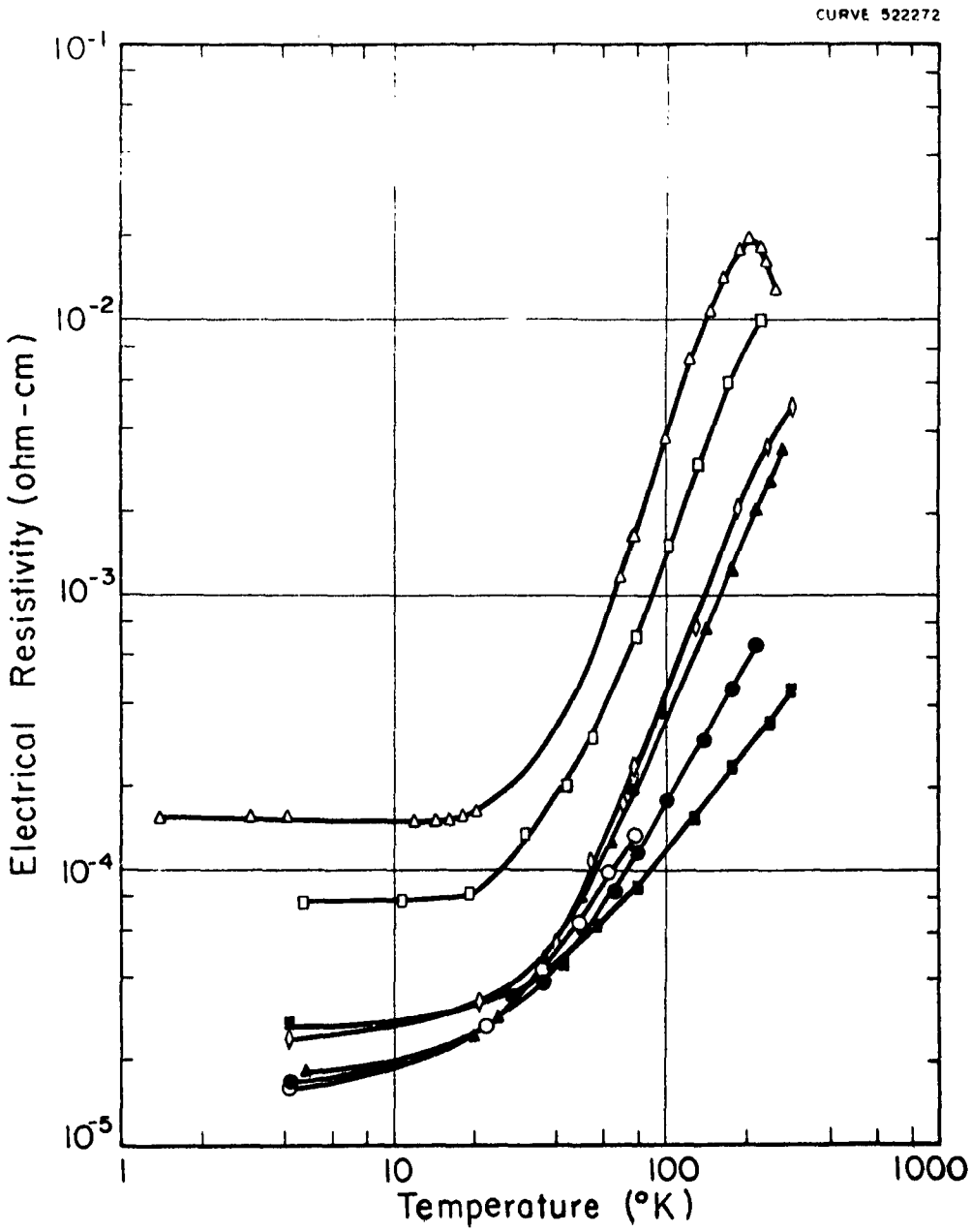

Fig. 4 - Resistivity of Te doped Bi_2Te_3

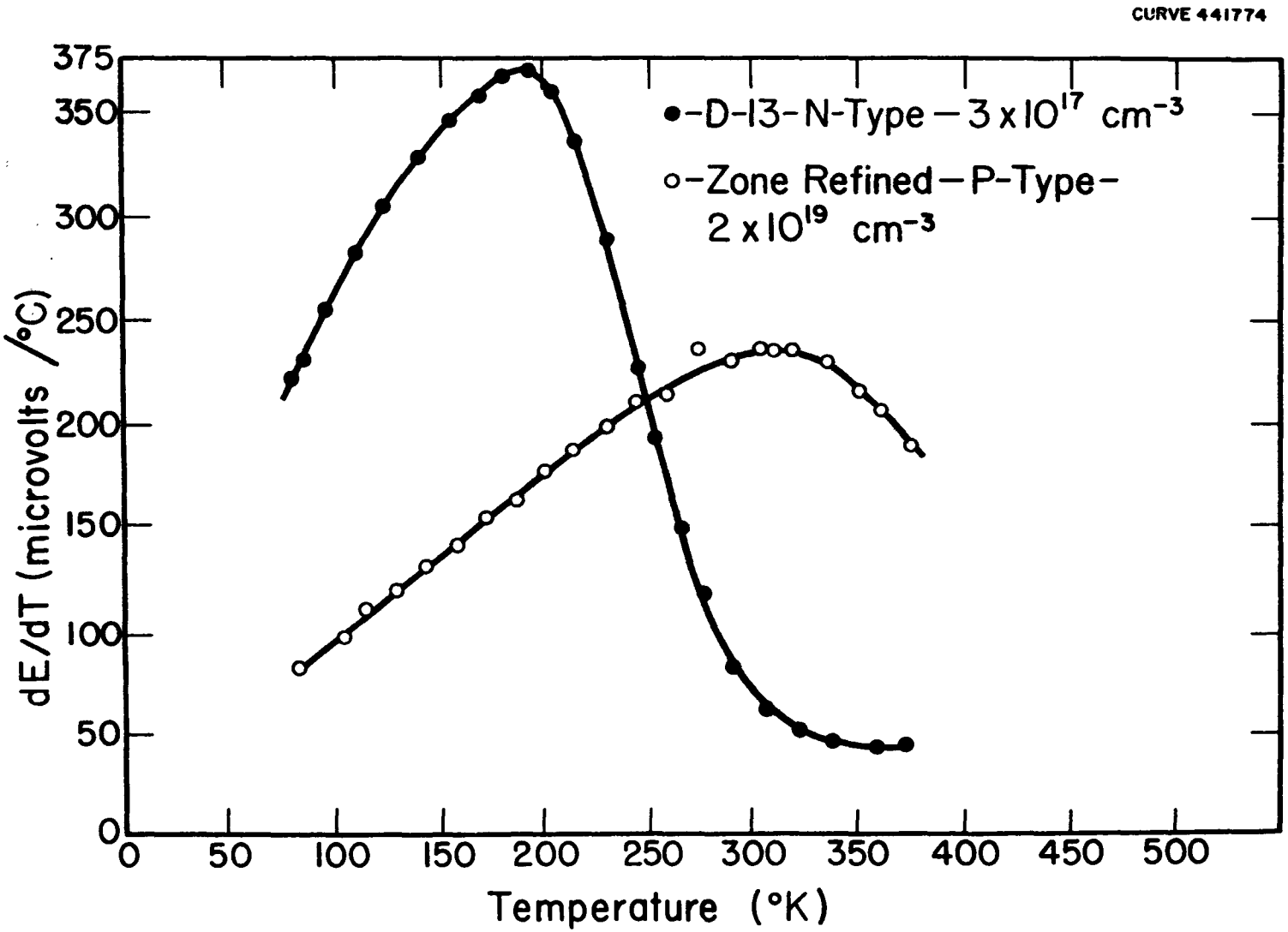

Fig. 5

CLM 23885

Scientific Paper 62-129-245-P3 May 2, 1962

THE TRANSPORT PROPERTIES OF BISMUTH SINGLE CRYSTALS

C. Gallo, B. S. Chandrasekhar and P.H. Sutter

To be submitted to the Journal of Applied Physics

Westinghouse Research Laboratories
Beulah Road, Churchill Borough
Pittsburgh 35, Pennsylvania

Scientific Paper 62-129-245-P3 May 2, 1962

THE TRANSPORT PROPERTIES OF BISMUTH SINGLE CRYSTALS

C. Gallo, B. S. Chandrasekhar and P. H. Sutter
Westinghouse Research Laboratories
Beulah Road, Churchill Borough
Pittsburgh 35, Pennsylvania

ABSTRACT

The absolute Seebeck coefficient, electrical resistivity, and thermal resistivity were simultaneously measured on pure bismuth single crystals of various orientations between approximately 80°K and 300°K. Using an overlapping two-band many-valley model, numerical values for the temperature dependence and anisotropy (where appropriate) of the following parameters have been calculated: (1) the overlap energy and the Fermi energy of the electrons and of the holes, (2) the density of states effective mass of the electron and of the holes, (3) the separate electronic and lattice thermal conductivities, (4) the actual index of thermoelectric efficiency, and the hypothetical "optimum" index of thermoelectric efficiency. The calculated electronic thermal conductivity includes a new term due to bipolar diffusion.

INTRODUCTION

Bismuth is a semimetal which has a crystal structure based on the rhombohedral lattice with two atoms per unit cell. Many of the electrical and thermal properties of bismuth are anisotropic and can be described with reference to the trigonal axis and three equivalent binary axes lying in a plane perpendicular to the trigonal axis.

The Jones' zone for bismuth can accommodate exactly five electrons per atom, so that there are just enough valence electrons to fill a band. However, there is an overlap in energy between the electron and hole bands and a small fraction of the electrons spill over into a higher zone, even at $0^{\circ}K$. Information concerning the band structure of bismuth has been obtained from measurements of the de Haas-van Alphen effect,[1-6] cyclotron resonance,[7-9] galvanomagnetic effects,[10-12] Seebeck coefficient,[13] piezoresistance,[14] magneto-optical effects,[15,16] ultrasonic attenuation[17] and anomalous skin effect.[18]

We have analyzed our measurements in terms of a parabolic two-band model. For both the electrons and holes, the constant energy surfaces are ellipsoids which are arranged in momentum space in accordance with the rhombohedral symmetry of the bismuth crystal. In our calculations, we have used Abeles and Meiboom's[10] results for the number of carriers and the mobility ratios. They used the following parabolic two-band model which is more specific than ours. The energy surfaces of the holes are spheroidal with the axis of revolution parallel to the trigonal axis of

the crystal. The energy surfaces of the electrons are ellipsoids, each one having one of its axes parallel to the trigonal axis and another axis parallel to the binary axis. De Haas-van Alphen effect,[1-4] cyclotron resonance[7-9] and other measurements[17,18] indicate that the electron ellipsoids are actually slightly tilted away from the trigonal plane. However, this should have a negligible effect on our results.

EXPERIMENTAL

Single crystals of about 0.2 cm^2 uniform cross-section and over 10 cm long were grown in a graphite mold in vacuum, using a modified Bridgman technique as previously described.[13] The bismuth, of 99.999% purity, was obtained from the American Smelting and Refining Company. Previous measurements[13] indicated that the Seebeck coefficient was essentially unaffected by zone refining, thus indicating a high degree of purity. Measurements on some crystals, as grown, indicated a ratio of room-temperature to liquid-helium-temperature resistivities of approximately ninety. Orientations close to the trigonal axis were obtained by suitable seeding. The orientations of the crystals were determined by back-reflection Laue photographs[19] and further checked by measuring the Seebeck coefficient (α) at 300°K and using a previously published[13] graph of α vs. orientation.

The samples were carefully cut to approximately 1 cm length with a jeweler's saw and the ends were lapped flat and parallel. The samples were etched in nitric acid and the ends were nickel plated. A low melting point alloy (Cerrolow 117) was used to solder the sample between the sample heater and cold plug of the apparatus shown in Fig. 1.

The apparatus of Fig. 1 was used to measure the electrical resistivity, thermal resistivity, and Seebeck coefficient of the sample. The temperatures were measured with copper-constantan thermocouples which were thermally bonded to isothermal regions before being

brought out of the apparatus. All of the measurements were made with a Leeds and Northrup K-3 potentiometer and appropriate standard resistors.

The isothermal electrical resistivity was measured by passing a dc current of about 0.1 amp through the sample. A reversing procedure was used to eliminate thermoelectric effects. The potential drop across the sample was measured across the copper leads of the thermocouples in the sample heater and cold plug. Thus, the measured resistance included the contact resistance of the soldered joints. In order to demonstrate that this contact resistance was small, tests were made on the assembled sample heater, sample, and cold plug before they were placed in the apparatus of Fig. 1. Room temperature resistivity measurements with a standard 4-probe ac apparatus[20] indicated that the contact resistance and inhomogeneity effects were less than 2%. Using an apparatus previously described,[21] potential profile measurements were also made on the assembled unit at room temperature. The linear nature of the curves indicated that the contact resistance was less than 2% of the sample resistance; that there were no cracks in the sample; and that the electrical properties were uniform along the length of the sample.

The Seebeck coefficient and thermal resistivity were measured by establishing a steady state temperature gradient across the sample and thermally matching the shield shown in Fig. 1. The Seebeck voltage was measured across the copper leads of the thermocouples. The absolute

Seebeck coefficient of bismuth was found by making a correction for the small absolute Seebeck coefficient of copper.[22] Simultaneously, the thermal resistivity was determined by measuring the power input to the sample heater. The stray heat losses[23] from the sample heater (mostly radiation) were determined as a function of temperature in a separate calibration run and appropriate corrections were made. The total correction, which included small corrections for the thermal contact resistance[23] (< 1%) and small temperature drifts[23] (< 1.5%), never exceeded 6%.

In order to verify that the effects of cold work were small in this temperature range, one sample was measured in the usual way and then was severely strained by bending. Remeasurement showed that the properties had changed by about 6% at 100°K.

RESULTS AND DISCUSSION

The absolute Seebeck coefficient (α), electrical resistivity (ρ) and thermal resistivity (r) were simultaneously measured between approximately 80°K and 300°K on six pure bismuth single crystals of various orientations. All of these properties are anisotropic. The rather large anisotropy of the thermal and electrical properties of bismuth is somewhat surprising since its crystal structure can be considered to be rhombohedral with only a slight distortion from cubic. Although the electrical and thermal resistivities are tensor quantities, it is convenient here to use the term "resistivity" to mean the measured resistance times area/length and "Seebeck coefficient" to mean the Seebeck voltage divided by the temperature difference. Then for the long thin rod geometry used here, both the electrical and thermal resistivity obey the Thomson-Voigt[24] relation as one would expect from the uniaxial symmetry associated with the rhombohedral structure:

$$R_\Phi = R_\perp + (R_{||} - R_\perp)\cos^2\Phi \qquad (1)$$

where R is either the thermal or electrical resistivity and Φ is the angle between the sample axis and the trigonal axis. The subscripts $||$ and $\perp$ denote directions parallel and perpendicular to the trigonal axis. Due to the anisotropy of the thermal conductivity, the absolute Seebeck coefficient shows a deviation from the Thomson-Voigt relation and obeys the equation[13, 25]

$$\alpha_\Phi = \alpha_\perp + \frac{\lambda(\alpha_{||} - \alpha_\perp)\cos^2\Phi}{1 + (\lambda-1)\cos^2\Phi} \qquad (2)$$

where $\lambda = K_{\perp}/K_{||}$, the ratio of the thermal conductivities perpendicular and parallel to the trigonal axis respectively. The measured values of ρ_{Φ} and r_{Φ} have been used to solve Eq. 1 by the method of least squares to obtain $\rho_{||}$, $\rho_{\perp}$, $r_{||}$ and $r_{\perp}$ as a function of temperature as shown in Figs. 2 and 3. Likewise, the measured values of α_{Φ} have been used to solve Eq.2 to obtain $\alpha_{||}$ and $\alpha_{\perp}$ as shown in Fig. 4. The least squares analysis for ρ, r and α gave a "standard error of estimate" which never exceeded 3%. All measurements are believed to be accurate to within $\pm 3\%$. The Seebeck coefficient measurements are in excellent agreement with those of Chandrasekhar.[13] The electrical resistivity measurements are in good agreement with those of other authors[10, 26, 27] who used methods which eliminated the electrical contact resistance problem. The thermal conductivity measurements are in good agreement with those of other authors,[27] although the temperature dependence of the present results appears to be somewhat slower at low temperatures.

In the following sections, several interesting parameters will be calculated:

(a) <u>The Overlap Energy, Fermi Energies and Density of States Effective Mass</u>

It has been previously shown[13] that

$$\alpha_i = \frac{(\sigma_e)_i \alpha_e + (\sigma_h)_i \alpha_h}{(\sigma_e)_i + (\sigma_h)_i} \qquad (3)$$

where i stands for $\|$ or $\perp$, σ is the electrical conductivity and the subscripts e and h refer to electrons and holes respectively. If the energy dependence of the relaxation time is independent of direction, then the partial Seebeck coefficients, α_e and α_h, are independent of direction. The anisotropy of α arises from the anisotropic and unequal carrier mobilities. Assuming parabolic bands, ellipsoidal energy surfaces, and that the energy dependence of the relaxation time is E^s, then[28]

$$\alpha_e = -\left(\frac{k}{e}\right) \frac{\left(\frac{5}{2} + s\right) F_{\left(\frac{3}{2} + s\right)}(\xi_e)}{\left(\frac{3}{2} + s\right) F_{\left(\frac{1}{2} + s\right)}(\xi_e)} - (\xi_e) \tag{4}$$

$$\alpha_h = +\left(\frac{k}{e}\right) \frac{\left(\frac{5}{2} + s\right) F_{\left(\frac{3}{2} + s\right)}(\xi_h)}{\left(\frac{3}{2} + s\right) F_{\left(\frac{1}{2} + s\right)}(\xi_h)} - (\xi_h) \tag{5}$$

where the Fermi integrals are given by

$$F_j(\xi) = \int_0^\infty \frac{x^j dx}{e^{x-\xi} + 1} \tag{6}$$

and the reduced Fermi energies are

$$\xi_e \equiv E_f^e/kT \qquad \xi_h \equiv E_f^h/kT = -\left(\frac{E_o + E_f^e}{kT}\right) \tag{7}$$

where E_f^e and E_f^h are the Fermi energies of the electrons and holes measured from the edges of their respective bands. The overlap energy, E_o, is measured from the top of the valence band to the bottom of the conduction band. For intra-valley acoustical mode lattice scattering, which is assumed in these calculations, s is - 1/2. Abeles and Meiboom[10] have calculated the anisotropic mobilities of the two types of carriers at 80°K and 300°K as shown in Table 1. From their data, the mobility ratios (μ_e/μ_h) appear to be very weakly temperature dependent. It was assumed that the individual mobilities parallel and perpendicular to the trigonal axis had the form $\mu = cT^y$. The results are very insensitive to this assumption. Using Abeles and Meiboom's data, we solved this equation for the constants* c and y and the mobility ratios were calculated at intermediate temperatures. With these values and the value of $\alpha_{||}$ and $\alpha_{\perp}$, Eq. 3 was solved for α_e and α_h as functions of temperature as shown in Fig. 5. The values of α_e and α_h were inserted into Eqs. 4 and 5 and ξ_e and ξ_h were obtained as a function of temperature by the use of tables of Fermi integrals. Using these values, we calculated the Fermi energies and the overlap energy from Eq. 7. The results are shown in Fig. 6. The equations and sign conventions used here are the same as those commonly used in the treatment of semiconductors. In our notation, E_o should be

---

* For both the electrons and holes, values of y of approximately -2.1 were found. The significance of this will be discussed later along with the scattering mechanism.

a negative number for the case of an overlap of the valence and conduction bands. The negative value found here is an independent determination that the conduction and valence bands overlap in bismuth. In other materials[29,30] where there is a question as to whether there is an energy gap or energy overlap, this method might be used to give a definite answer. The overlap energy is a sensitive function of temperature as shown in Fig. 6. This is not unexpected since E_o depends on the lattice spacing which is temperature sensitive through thermal expansion. Also, it is well known that the energy gap in semiconductors is generally a function of temperature.

The total number (N) of electrons (or holes) per unit volume has been calculated by Abeles and Meiboom[10] at 80°K and 300°K as shown in Table 1. Assuming that the bands are parabolic[28]

$$N = \left(\frac{4\pi}{h^3}\right)(2m_o kT)^{3/2}(m^*_T)^{3/2}F_{1/2}(\xi) \qquad (8)$$

where m^*_T is defined by Eq. 8 and may be called the "total density of states effective mass" in units of m_o. This parameter, which is isotropic and independent of the number of ellipsoids, has been calculated at 80°K and 300°K (Tables 2 and 3) using the values of ξ and N. This parameter will be of interest in discussing the thermoelectric efficiency later on. Similarly, the density of states effective masses "per ellipsoid" for the electrons and holes were calculated at 80°K and 300°K (Tables 2 and 3) from the equation

$$\left(\frac{N}{n}\right) = \left(\frac{4\pi}{h^3}\right)(2m_o kT)^{3/2}(m^*)^{3/2}F_{1/2}(\xi) \qquad (9)$$

where n is the number of ellipsoids, N/n is the number of electrons or holes per ellipsoid per unit volume, and m^* is the density of states effective mass per ellipsoid in units of m_o. In this approach, n is a variable interger. This m^* corresponds to the effective mass which is derived from the de Haas-van Alphen effect, cyclotron resonance and other methods. These measurements determine the components of the reciprocal mass tensor of an individual ellipsoid, but do not readily yield information concerning the number of ellipsoids.

Electrons: The Fermi energy of the electrons has been determined by Shoenberg[1-3] from de Haas-van Alphen effect measurements. The present results (Fig. 6) are in excellent agreement with his value of $E_f^e = 0.0177$ ev at 4^oK. The density-of-states effective mass of the electrons per ellipsoid has been calculated from the components of the effective mass tensor as determined by other methods.[7,9,17,18] All of these other measurements were made at liquid helium temperatures. Table 2 presents the results; where necessary, the value of E_f^e was assumed to be 0.0177 ev. The density-of-states effective mass per ellipsoid that is determined by the present work depends on whether a 3 or 6 ellipsoid model is assumed. As can be seen from Table 2, both values are in reasonable quantitative agreement with the other measurements. We are unable to choose between 3 or 6 ellipsoids

because of the divergence of the other results. From the present results (Table 2), it appears that the density-of-states effective mass of the electrons is independent of temperature between 80°K and 300°K. This indicates that the electron band is parabolic.[31]

Holes: The Fermi energy of the holes has been determined by Brandt[6] from de Haas-van Alphen effect measurements. Our low temperature results agree withhis value of $E_f^h = 0.0156$ ev. Brandt[6] has also found $m^*_h = 0.115\ m_o$, which is in excellent agreement with our low temperature value that was calculated assuming one hole spheroid (Table 3). This agreement is evidence that the energy surface for the holes is described by only one spheroid.[32] From anomalous skin effect measurements and with the assumption that there are two hole spheroids, Smith[18] has found values of the components of the reciprocal mass tensor divided by the Fermi energy. Using Brandt's value of $E_f^h = 0.0156$ ev with Smith's data, one finds $m^*_h \sim 0.1\ m_o$.

From low temperature specific heat measurements,[18,33] estimates of $m^*_h \cong 1\ m_o$ and $E_f^h \cong 0.001$ ev have been made. Recent galvanomagnetic and thermomagnetic experiments by Sybert, Grenier and Reynolds[34] indicate the existence of two hole bands. The uppermost valence band has a high mobility and presumably a low effective mass. The lower valence band has a lower mobility and presumably a higher effective mass. Thus it

seems reasonable that the "dominant" hole band has a light effective mass as found by Galt, et al.,[7] Chandrasekhar,[13] Brandt[6] and Smith[18] (as modified above). Presumably then, it is this lower heavy-mass band which contributes to the specific heat. Also, this additional band may be the cause of the temperature dependence of m^*_h which we have observed. From the temperature dependence of E^h_f (Fig. 6), it seems that this extra hole band plays a role in the transport properties above approximately $200^\circ K$.

Scattering Mechanism: Our results are sensitive to the assumption of intra-valley carrier scattering by acoustical mode lattice waves ($s = -1/2$). Although they are not presented, we have also done the calculations assuming that $s = +1/2$. However, the Fermi energies of both the electrons and holes as determined by the de Haas-van Alphen measurements[1-3,6] are in agreement with our results only if a value of $s = -1/2$ is assumed. Thus, at low temperatures, it appears that both the electrons and holes are predominantly scattered by acoustical mode lattice waves as one would expect. For such a case, theory predicts $\mu = cT^{-1.5}$. As previously described, however, we have found $\mu \cong cT^{-2.1}$ from Abeles and Meiboom's data. This discrepancy is probably due to the effect of the second valence band. However, it may also be due to non-parabolic hole band(s), the onset of optical mode lattice scattering or inter-valley effects. In any event, our treatment does not take these higher temperature effects into account.

(b) The Electronic and Lattice Thermal Conductivities

It was assumed that the measured thermal conductivity is the sum of the lattice thermal conductivity (K_L) and the total electronic thermal conductivity (K_E).

$$K = K_L + K_E \tag{10}$$

For the present model,* the total electronic thermal conductivity is given by the sum of three terms:[35] (1) the ordinary thermal conductivity due to electrons alone, κ_e, (2) the ordinary thermal conductivity due to holes alone, κ_h, and (3) the transport of heat due to bipolar diffusion, κ_{eh}.

$$K_E = \kappa_e + \kappa_h + \kappa_{eh} \tag{11}$$

The ordinary thermal conductivities have been extensively treated in the literature.[28] However, the bipolar diffusion term for the case of a semi-metal with overlapping bands has only recently been realized[35]— although the analogous situation in semiconductors is well known. Briefly this term is present for the following reason. The thermal conductivity is defined as the heat flux divided by the temperature

---

* As previously discussed, there really appear to be more than two active bands in bismuth. Therefore, there will be other terms in K_E. However, these extra terms will be small and we have done the calculations on the two-band model.

gradient when the total electrical current is zero. The ordinary terms give the heat flow contributions of the electrons and holes separately when their individual electrical currents are zero. For materials with carriers of both signs, there is an additional term which arises because the individual electrical currents are not zero although the total electrical current is zero. This effect may be thought of as the transport of the "heat of formation" of electron-hole pairs which diffuse from the hot region to the cold. From our previous calculations, it is possible to evaluate all three terms, which are[28,35]

$$K_E = T\left(\frac{k}{e}\right)^2\left[\gamma(\xi_e)\sigma_e + \gamma(\xi_h)\sigma_h\right] + T\left(\frac{\sigma_e\sigma_h}{\sigma}\right)(\alpha_h - \alpha_e)^2 \qquad (12)$$

where

$$\gamma(\xi) = \frac{(s + 7/2)F_{s + 5/2}(\xi)}{(s + 3/2)F_{s + 1/2}(\xi)} - \left[\frac{(s + 5/2)F_{s + 3/2}(\xi)}{(s + 3/2)F_{s + 1/2}(\xi)}\right]^2 . \qquad (13)$$

The results for the principal directions are shown in Figs. 3, 7 and 8.

The values of $\left(\frac{k}{e}\right)^2\gamma(\xi)$ that were found from Eq. 13 and used in calculating κ_e and κ_h are shown in Table 4. These values of $\kappa_e/\sigma_e T$ and $\kappa_h/\sigma_h T$ are considerably different from the "usual Lorenz Number" of $2.45 \times 10^{-8}(\text{volts}/^\circ\text{C})^2$, which only holds in the degenerate approximation. The carriers in bismuth must be described by the exact Fermi-Dirac statistics and, in such a case, $\gamma(\xi)$ is a function of the Fermi level and the scattering mechanism as is given in Eq. 13. The energy

dependence of the relaxation time has been assumed to be independent of direction, which implies that $\gamma(\xi)$ is isotropic. In Table 4, it can be seen that $\gamma(\xi_e) = \gamma(\xi_h)$. Thus, letting $\gamma = \gamma(\xi_e) = \gamma(\xi_h)$, Eq. 12 can rewritten as

$$\frac{K_E}{\sigma T} = \left(\frac{k}{e}\right)^2 \gamma + \left(\frac{\sigma_e \sigma_h}{\sigma^2}\right)(\alpha_h - \alpha_e)^2 \qquad (14)$$

In order to compare our results with earlier measurements on bismuth crystals, the "pseudo-Lorenz Number," L, has been calculated from our data as shown in Table 4. This quantity, which presumably is the one determined experimentally in the work discussed below, is defined as

$$L \equiv \frac{K_E}{\sigma T} \qquad (15)$$

Now, if the bipolar term were not present in Eq. 14, L would be isotropic. However, from magnetoresistance and magneto-thermal conductivity measurements, Gruneisen and Gielessen[36] have found that L is anisotropic. The bipolar term (κ_{eh}) provides such an anisotropic contribution to L because the factor $\sigma_e\sigma_h/\sigma^2$ is anisotropic. The qualitative agreement between the present calculations and Gruneisen and Gielessen's measurements is strong evidence for the existence of the bipolar contribution to the electronic thermal conductivity.

The magnetoresistance and magneto-thermal conductivity measurements of Gruneisen, Rausch and Weiss[37] at 80°K perpendicular to the trigonal axis, yield a value of L in reasonable agreement with our results. It is very interesting that the value of L found by Gruneisen, Rausch and Weiss, as well as some of those calculated here (Table 4), are close to the "usual Lorenz Number" -- a pure accident! The agreement is merely due to the fortuituous combination of the bipolar term and the ordinary terms properly derived with exact Fermi-Dirac statistics. The values of L obtained by de Haas, Gerritsen and Capel[38] by saturation magneto-thermal conductivity measurements at 80°K parallel to the trigonal axis are not in agreement with our calculations. However, their particular type of measurement may not be considered a satisfactory method of separating out the electronic thermal conductivity. In view of the present situation, careful experimental and theoretical treatments of magnetoresistance and magneto-thermal conductivity would be valuable, particularly at high fields.

The lattice thermal conductivity was calculated from Eq. 10 for each of the principal directions. The lattice thermal resistivity, which is the scalar reciprocal of the conductivity for the principal directions, is shown in Fig. 9 as a function of temperature.

Theoretically, the lattice thermal conductivity is given roughly by

$$K_L \cong 1/3\ cv\lambda \qquad (16)$$

where c is the lattice specific heat per unit volume, v is the velocity of sound and λ is the phonon mean free path. The lattice specific heat of bismuth is approximately given by the Debye theory with a Debye temperature (θ) of 120°K. The velocity of sound[39] is essentially independent of temperature and it is anisotropic, which at least in part accounts for the anisotropy of the lattice thermal conductivity. For an isotropic solid above the Debye temperature, Ioffe[40] has recently proposed that for phonon-phonon Umklapp scattering that

$$\frac{1}{\lambda} = A \int_0^T c\,dT \qquad (17)$$

where A is a constant for a given material. The phonon mean free path at each temperature was roughly calculated from Eq. 16 for the principal directions. The temperature dependence of λ obtained in this way was found to follow Eq. 17 within the rather poor precision of the comparison. Above the Debye θ, the temperature dependence of the lattice thermal resistivity is essentially contained in the $1/\lambda$ factor. At these temperatures, c is nearly constant and it can be shown that the integral in Eq. 17 is proportional to $(T - \theta/3)$. Thus, above the Debye θ, Ioffe[40] proposes that the lattice thermal resistivity should approach

$$r_L \propto (T - \theta/3) \quad . \qquad (18)$$

According to Eq. 18, a plot of lattice thermal resistivity versus absolute temperature should approach a straight line which should extrapolate back to $T = \theta/3$. From Fig. 9, it can be seen that our results are in better agreement with Eq. 18 than with older theories which predict that for $T > \theta$, the lattice thermal resistivity should extrapolate to zero at $0^{\circ}K$. However, the agreement with Ioffe's theory is only qualitative. As one would expect from Ioffe's ideas, there is a deviation from Eq. 18 in Fig. 9 around the Debye temperature.

(c) Thermoelectric Efficiency

The thermoelectric "index of efficiency" (ZT) is given by[28]

$$ZT = \left(\frac{\alpha^2}{\rho K}\right)T \tag{19}$$

This parameter, which has been calculated for the two principal orientations from our data, is shown in Fig. 10. For real bismuth, the maximum value of Z occurs parallel to the trigonal axis.[41]

Since the macroscopic parameter Z is a sensitive function of the carrier concentrations, it is convenient to speak of a "hypothetical optimum index of efficiency" (Z_oT). Briefly, Z_o occurs when only one type of carrier is present and the Fermi level is adjusted to yield an optimum value of Z. The presence of only one type of carrier ensures that the Seebeck coefficient (Eq. 3) is a

maximum and that thermal conduction by bipolar diffusion is essentially zero. It can be shown[28] that Z_oT is a monotonically increasing function of the microscopic material parameter (β) defined as

$$\beta = \left(\frac{T}{300}\right)^{5/2}\left(\frac{m^*_T}{m_o}\right)^{3/2}\left(\frac{\mu_c}{K_L}\right) \tag{20}$$

where μ_c is the classical carrier mobility, which is related to the actual mobility by the relation

$$\mu_c = \mu \frac{(s + 1/2)!F_{1/2}(\xi)}{(1/2)!F_{(s + 1/2)}(\xi)} \quad . \tag{21}$$

From the data previously discussed and Eqs. 20 and 21, β has been calculated assuming that μ_c, m^*_T, and K_L are unchanged in meeting the physical requirements mentioned above. Knowing β, the hypothetical "optimum" index of efficiency (Z_oT) was obtained from graphs published by Ure.[28] The results for the two principal orientations are shown in Fig. 11 for N-type material. The results for P-type material do not look promising and are not presented.

The anisotropy of Z_oT ($\sim$1.6:1) arises from the anisotropic nature of the ratio μ_e/K_L. In addition to the anisotropy of μ_e/K_L, the larger anisotropy of ZT ($\sim$6.5:1) in real bismuth is due to the anisotropy of the absolute Seebeck coefficient and thermal conduction by bipolar diffusion. The anisotropy in α and κ_{eh} is, in turn, due to the anisotropy in the mobility ratios, μ_e/μ_h.

The Z of real bismuth is considerably below Z_o primarily because of the presence of the holes which adversely effect α and K_E. Also, the electron concentration is too high to give the optimum Z. By suitable alloying with antimony ($\sim$10%), the bands can be separated and a discrete energy gap introduced.[42] With appropriate N-type doping, the deleterious effect of the holes can be minimized and the electron concentration can be adjusted to yield an optimum Z. Experiments of this type by Smith and Wolfe[43] indicate that reasonably high values of ZT can be obtained. In fact, it is conceivable that a Bi-Sb alloy with suitable doping may yield a value of ZT higher than the Z_oT shown in Fig. 11. Due to the difference in the phonon and electron wavelengths, scattering by Sb atoms may lower K_L more than μ_e and thus increase the ratio μ_e/K_L and Z_oT. This argument[44] will be particularly true at low temperatures, and indeed, this appears to be the case experimentally.[43]

It has been argued[45] that anisotropic semiconductors may be a promising area for the search of thermoelectric materials in spite of the fact that the high mobility direction will probably coincide with the high lattice thermal conductivity direction. In bismuth, at least, the high electron mobility direction coincides with the low lattice thermal conductivity direction. This fact makes the search for good thermoelectric materials among anisotropic materials seem all the more promising.

SUMMARY

Our measurements have been analyzed in terms of a parabolic two-band multi-valley model, where the two bands overlap. However, other recent work[12,34] indicates that there really are two hole bands. This, together with the present results, indicates that:

(1) The electrons are described by one band with either three or six ellipsoids. The electron band is parabolic.

(2) There are two non-degenerate hole bands.[34] The higher band, which is dominant at low temperatures, is described by a single spheroid with a high mobility,[10] a low density of states effective mass[6,7,13] ($m_h^* \cong 0.1\ m_o$), and a Fermi energy[6] comparable to that of the electrons ($E_f^h \cong 0.016$ ev at 80^oK). The lower hole band[34] has a lower mobility, a higher density of states effective mass, and a lower Fermi energy.

(3) The magnitude of the energy overlap between the electron band and the highest hole band is an increasing function of temperature. Thus the Fermi energies are a function of temperature.

(4) The electrons and holes are predominantly scattered by acoustical mode lattice waves at low temperatures.

(5) The transport properties of bismuth can be treated with the equations developed for semiconductors, provided that exact Fermi-Dirac statistics are used. There are undoubtedly other semi-metals which can be successfully treated with the present methods.

(6) In bismuth, there is a sizeable additional term in the electronic thermal conductivity due to bipolar diffusion. Up till now, this effect has been overlooked. Between 100°K and 300°K, thermal conduction by electrons and holes is the dominant mechanism.

(7) The temperature dependence of the lattice thermal resistivity is better described by the recent ideas of Ioffe than by older theories which predict an extrapolation to zero at 0°K.

(8) From the experiments of Smith and Wolfe[43] and from this study of pure bismuth, it appears that Bi-Sb alloys with appropriate doping will be of practical thermoelectric interest. In bismuth, the high electron mobility direction coincides with the low lattice thermal conductivity direction. This fact makes the search for good thermoelectric materials among anisotropic semiconductors and semimetals seem all the more promising.

ACKNOWLEDGEMENTS

We are glad to thank Dr. R. W. Ure, Jr. for many valuable discussions on the band theory of solids, Dr. J. E. Bauerle for the design of the original equipment, and Dr. P. G. Klemens for discussions of the lattice thermal conductivity. We are also indebted to P. Piotrowski, R. Aufinger, and B. Kagle for assistance with some of the sample preparations and measurements. This work has been partially supported by the Bureau of Ships.

Table 1. The number and mobility of electrons and holes in bismuth according to Abeles and Meiboom.[10] N = P is the number of electrons or holes per cm^3. The μ's denote mobilities in cm^2 $statvolt^{-1}$ sec^{-1}. The subscripts e and h denote electrons and holes respectively, and the subscripts $||$ and $\perp$ indicate directions parallel and perpendicular to the trigonal axis respectively.

	300°K	80°K
N, P x 10^{-18}	2.2	.46
$(\mu_e)_{||}$ x 10^{-6}	5.7	100.
$(\mu_e)_{\perp}$ x 10^{-6}	4.87	85.6
$(\mu_h)_{||}$ x 10^{-6}	.62	10.
$(\mu_h)_{\perp}$ x 10^{-6}	2.3	37.
$(\mu_e/\mu_h)_{||}$	9.19	10.0
$(\mu_e/\mu_h)_{\perp}$	2.12	2.31

Table 2. Electrons: Density of states effective mass in units of m_o

Method	~ 4°K	80°K	300°K
Present work - Total (1 Spheroid)		.113	.113
3 Ellipsoids		.054	.054
6 Ellipsoids		.034	.034
Cyclotron resonance with Shoenberg's[1-3] de Haas-van Alphen measurements (Aubrey)[9]	.042		
Cyclotron resonance (Galt et al.)[7]	.052		
Anomalous skin effect with specular reflection assuming six ellipsoids and E_f^e =0.0177 ev (Smith)[18]	.042		
Ultrasonic attenuation assuming E_f^e =0.0177 ev (Reneker)[17]	.051		

Table 3. Holes: Density of states effective mass in units of m_o

Method	~ 4°K	80°K	300°K
Present work - Total (1 Spheroid)		.120	.093
2 Spheroids		.076	.059
de Haas-van Alphen effect (Brandt)[6]	.115		
Cyclotron Resonance (Galt et al.)[7]	.162		
Anomalous skin effect with specular reflection assuming two spheroids and E_f^h = 0.0156 ev (Smith)[18]	.099		

Table 4. The ratio of the carrier contributions to the thermal and electrical conductivities. Equation 13 was used to calculate $\kappa_e/\sigma_e T = (\frac{k}{e})^2 \gamma(\xi_e)$ and $\kappa_h/\sigma_h T = (\frac{k}{e})^2 \gamma(\xi_h)$. Values for the "pseudo-Lorenz number," $L = K_E/\sigma T$, were calculated from Eqs. 12 and 13 and include the bipolar term of the total electronic thermal conductivity.

$T(^oK)$	$\kappa_e/\sigma_e T$ $(v/^oC)^2$	$\kappa_h/\sigma_h T$ $(v/^oC)^2$	$L_{\parallel} = \left(\frac{K_E}{\sigma T}\right)_{\parallel}$ $(v/^oC)^2$	$L_{\perp} = \left(\frac{K_E}{\sigma T}\right)_{\perp}$ $(v/^oC)^2$
100	1.85×10^{-8}	1.84×10^{-8}	2.30×10^{-8}	2.98×10^{-8}
150	1.79	1.75	2.42	3.35
200	1.78	1.74	2.45	3.44
250	1.79	1.79	2.38	3.26
300	1.81	1.88	2.29	3.00

REFERENCES

1. D. Shoenberg, Proc. Roy. Soc. (London) A170, 341 (1939).

2. D. Shoenberg, Phil. Trans. Roy. Soc.(London) A245, 1 (1952).

3. J. S. Dhillon and D. Shoenberg, Phil. Trans. Roy. Soc. (London) A248, 1 (1955).

4. D. Shoenberg, Progress in Low Temperature Physics, edited by C. J. Gorter (Interscience, New York, 1957), Vol. 2, Chap. 8.

5. N. B. Brandt, A. E. Dubrovskaya and G. A. Kytin, Soviet Physics--JETP 10, 405 (1960).

6. N. B. Brandt, Soviet Phys.--JETP 11, 975 (1960).

7. J. K. Galt, W. A. Yager, F. R. Merritt, B. B. Cetlin and A. D. Brailsford, Phys. Rev. 114, 1396 (1959).

8. J. E. Aubrey and R. G. Chambers, J. Phys. Chem. Solids 3, 128 (1957).

9. J. E. Aubrey, J. Phys. Chem. Solids 19, 321 (1961).

10. B. Abeles and S. Meiboom, Phys. Rev. 101, 544 (1956).

11. R. A. Connell and J. A. Marcus, Phys. Rev. 107, 940 (1957).

12. K. Tanaka, S. Tanuma and T. Fukuroi, Sci. Repts. Tohoku Univ. A13, 67 (1961).

13. B. S. Chandrasekhar, J. Phys. Chem. Solids 11, 268 (1959).

14. R. W. Keyes, Phys. Rev. 104, 665 (1956).

15. B. Lax, J. G. Mavroides, H. J. Zeiger and R. J. Keyes, Phys. Rev. Letters 5, 241 (1960).

16. R. N. Brown, J. G. Mavroides, M. S. Dresselhaus and B. Lax, Phys. Rev. Letters 5, 243 (1960).

17. D. H. Reneker, Phys. Rev. 115, 303 (1959).

18. G. E. Smith, Phys. Rev. 115, 1561 (1959).

19. W. Vickers, Trans. Am. Inst. Mining, Met., Petrol. Engrs. 209, 827 (1957).

20. R. W. Ure, Jr., Thermoelectricity - Science and Engineering, edited by R. R. Heikes and R. W. Ure, Jr. (Interscience, New York, 1961). pp. 322-326.

REFERENCES (continued)

21. P. H. Sutter, Reference 20, pp. 334-336.

22. N. Cuscak and P. Kendall, Proc. Phys. Soc. (London) 72, 898 (1958).

23. J. E. Bauerle, Reference 20, pp. 287-289, 292-295, 296, 297.

24. J. F. Nye, Physical Properties of Crystals (Oxford University Press, London, 1960), pp. 24-26, 195-200, 204-207.

25. M. Kohler, Ann. Physik 40, 196 (1941).

26. For a convenient summary, see A. N. Gerritsen, Encyclopedia of Physics, edited by S. Flügge (Springer-Verlag, Berlin, 1956), Vol. 19, Electrical Conductivity, pp. 157, 158, 173.

27. For a convenient summary, see R. L. Powell and W. A. Blanpied, Thermal Conductivity of Metals and Alloys at Low Temperatures, NBS Circular 556, (1954), pp. 36, 37, 54.

28. These equations and concepts are discussed by R. W. Ure, Jr., Thermoelectricity - Science and Engineering, edited by R. R. Heikes and R. W. Ure, Jr. (Interscience, New York, 1961), Chaps. 3 and 11.

29. A. Sagar and R. C. Miller, Bull. Am. Phys. Soc. 7, 203 (1962).

30. R. F. Brebrick and A. J. Strauss, Bull. Am. Phys. Soc. 7, 203 (1962).

31. M. H. Cohen, Phys. Rev. 121, 387 (1961).

32. G. E. Smith, J. Phys. Chem. Solids 20, 168 (1961).

33. N. E. Philips, Phys. Rev. 118, 644 (1960).

34. J. R. Sybert, C. G. Grenier and J. M. Reynolds, Bull. Am. Phys. Soc. 7, 74 (1962).

35. C. Gallo, R. C. Miller, P. H. Sutter and R. W. Ure, Jr., To be submitted to J. Appl. Phys.

36. E. Gruneisen and J. Gielessen, Ann. Physik 26, 449 (1936).

37. E. Gruneisen, K. Rausch and K. Weiss, Ann. Physik 7, 1 (1950).

38. W. J. de Haas, A. N. Gerritsen and W. H. Capel, Physica 3, 1143 (1936).

39. Y. Eckstein, A. W. Lawson and D. H. Reneker, J. Appl. Phys. 31, 1534 (1960).

40. A. F. Ioffe, Physics of Semiconductors (Academic Press, New York, 1960), pp. 274-281.

REFERENCES (continued)

41. S. V. Airapetyants, Soviet Phys.--Solid State 3, 2093 (1962).

42. A. L. Jain, Phys. Rev. 114, 1518 (1959).

43. G. E. Smith and R. Wolfe, J. Appl. Phys. 33, 841 (1962).

44. A. F. Ioffe, S. V. AirapetYants, A. V. Ioffe, N. V. Kolomoets and L. S. Stilbans, Doklady Akad. Nauk S.S.S.R. 106, 981 (1956).

45. R. W. Ure, Jr., Reference 28, pp. 355-357.

FIGURE CAPTIONS

Fig. 1. Schematic diagram of the apparatus for measuring α, ρ and K. The sample was soldered between the sample heater and the cold plug. For Seebeck coefficient and thermal resistivity measurements, the temperature of the thermal shield was matched to that of the sample heater. The parts shown were suspended and evacuated to 10^{-5} mm Hg in a can which was placed in an appropriate low temperature bath. The overall temperature was adjusted with a heater in the heat sink.

Fig. 2. Electrical resistivity vs. temperature for pure bismuth single crystals; $\rho_{||}$ and $\rho_{\perp}$ were calculated by fitting Eq. 1 to the data.

Fig. 3. The total measured thermal conductivity (K) and the total calculated electronic thermal conductivity (K_E) vs. temperature for pure bismuth single crystals. $K_{||} = \frac{1}{r_{||}}$ and $K_{\perp} = \frac{1}{r_{\perp}}$ were calculated by fitting Eq. 1 to the data. $(K_E)_{||}$ and $(K_E)_{\perp}$ were calculated from Eqs. 11-13.

Fig. 4. Absolute Seebeck coefficient vs. temperature for pure bismuth single crystals; $\alpha_{||}$ and $\alpha_{\perp}$ were calculated by fitting Eq. 2 to the data.

FIGURE CAPTIONS (continued)

Fig. 5. The isotropic partial Seebeck coefficient of the electrons (α_e) and holes (α_h) vs. temperature for pure bismuth single crystals. The dotted lines are extrapolated to zero at $0^{\circ}K$.

Fig. 6. The overlap energy (E_o) and the Fermi energy of the electrons (E_f^e) and holes (E_f^h) vs. temperature for pure bismuth single crystals.

Fig. 7. The individual contributions to the total electronic thermal conductivity (K_E) for pure bismuth single crystals perpendicular to the trigonal axis. The ordinary thermal conductivity due to electrons alone (κ_e), the ordinary thermal conductivity due to holes alone (κ_h), and the thermal conductivity due to bipolar diffusion (κ_{eh}) were calculated from Eqs. 11-13. For this orientation, $(\mu_e/\mu_h)_\perp \cong 2$.

Fig. 8. The individual contributions to the total electronic thermal conductivity (K_E) for pure bismuth single crystals parallel to the trigonal axis. The ordinary thermal conductivity due to electrons alone (κ_e), the ordinary thermal conductivity due to holes alone (κ_h), and the thermal conductivity due to bipolar diffusion (κ_{eh}) were calculated from Eqs. 11-13. For this orientation, $(\mu_e/\mu_h)_{||} \cong 10$.

FIGURE CAPTIONS (continued)

Fig. 9. The calculated lattice thermal resistivity vs. temperature for pure bismuth single crystals. The scatter at the higher temperatures is due to the fact that the lattice thermal conductivity is the difference between two large numbers in Eq. 10 as can be seen in Fig. 3.

Fig. 10. The index of thermoelectric efficiency vs. temperature for pure bismuth single crystals.

Fig. 11. The hypothetical optimum index of thermoelectric efficiency vs. temperature for "optimized N-type bismuth crystals."

DWG. 624A269

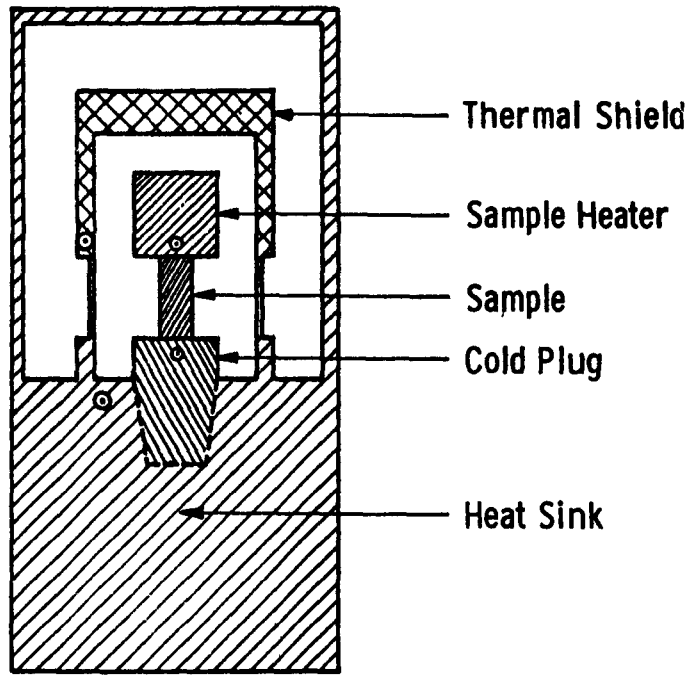

⊙ Denote Cu-Const Thermocouples

Fig. 1

Schematic diagram of the apparatus for measuring α, ρ and K. The sample was soldered between the sample heater and the cold plug. For Seebeck coefficient and thermal resistivity measurements, the temperature of the thermal shield was matched to that of the sample heater. The parts shown were suspended and evacuated to 10^{-5}mm Hg in a can which was placed in an appropriate low temperature bath. The overall temperature was adjusted with a heater in the heat sink.

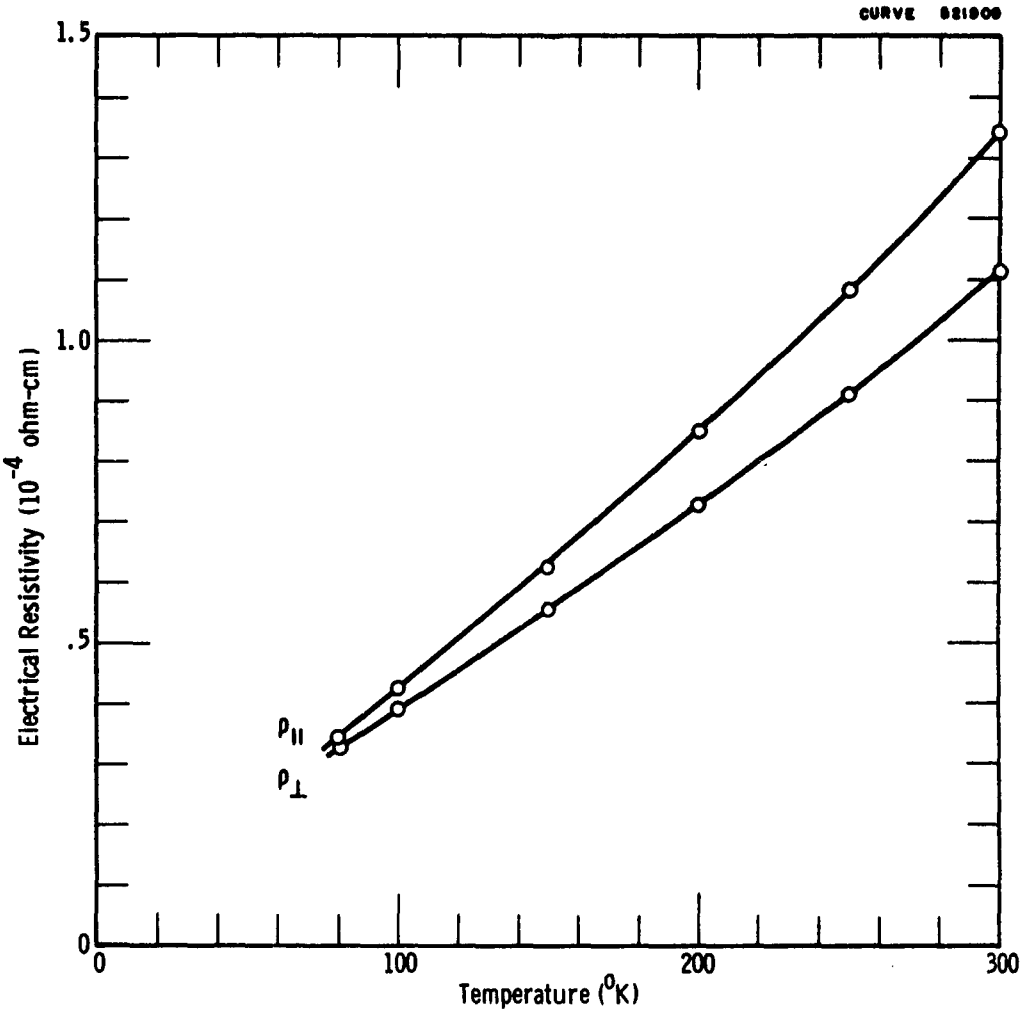

Fig. 2

Electrical resistivity vs. temperature for pure bismuth single crystals; $\rho_{||}$ and $\rho_{\perp}$ were calculated by fitting Eq. 1 to the data.

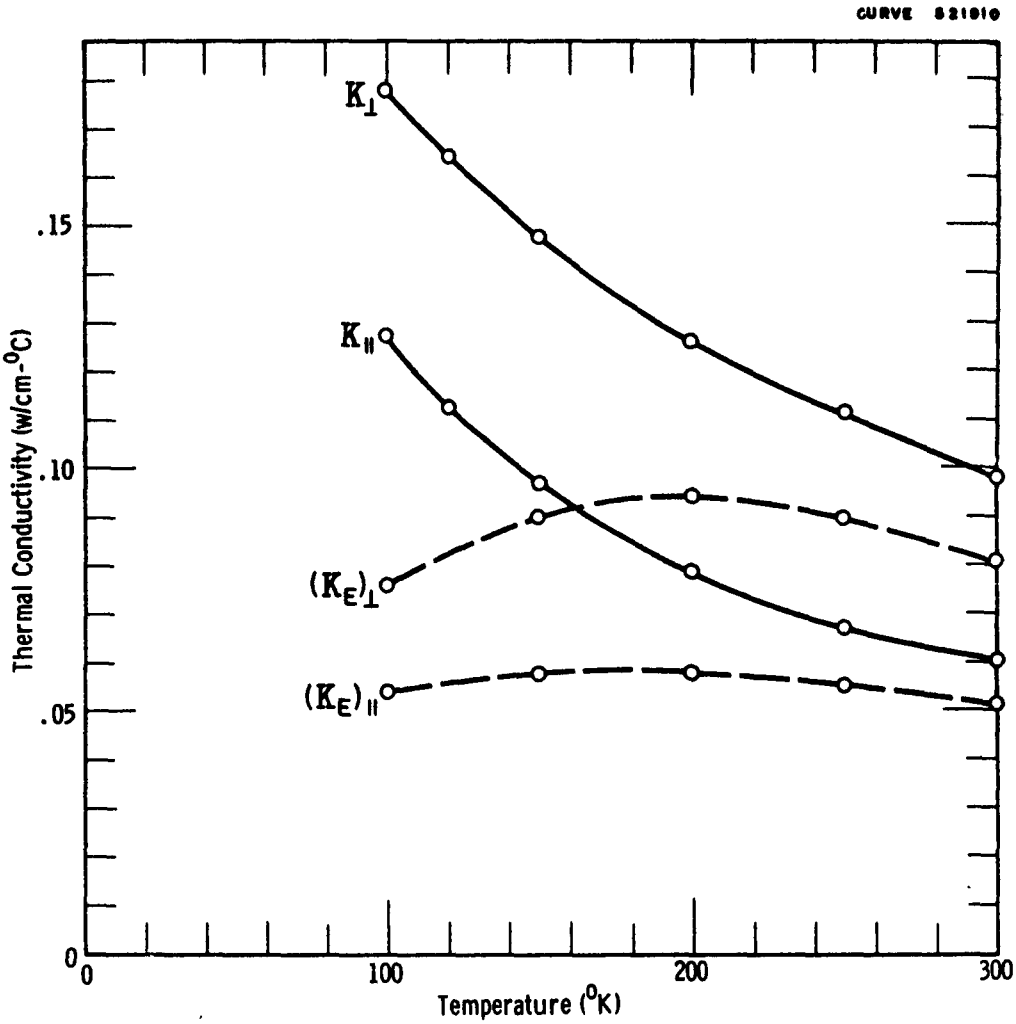

Fig. 3

The total measured thermal conductivity (K) and the total calculated electronic thermal conductivity (K_E) vs. temperature for pure bismuth single crystals. $K_{||} = \frac{1}{r_{||}}$ and $K_\perp = \frac{1}{r_\perp}$ were calculated by fitting Eq. 1 to the data. $(K_E)_{||}$ and $(K_E)_\perp$ were calculated from Eqs. 11-13.

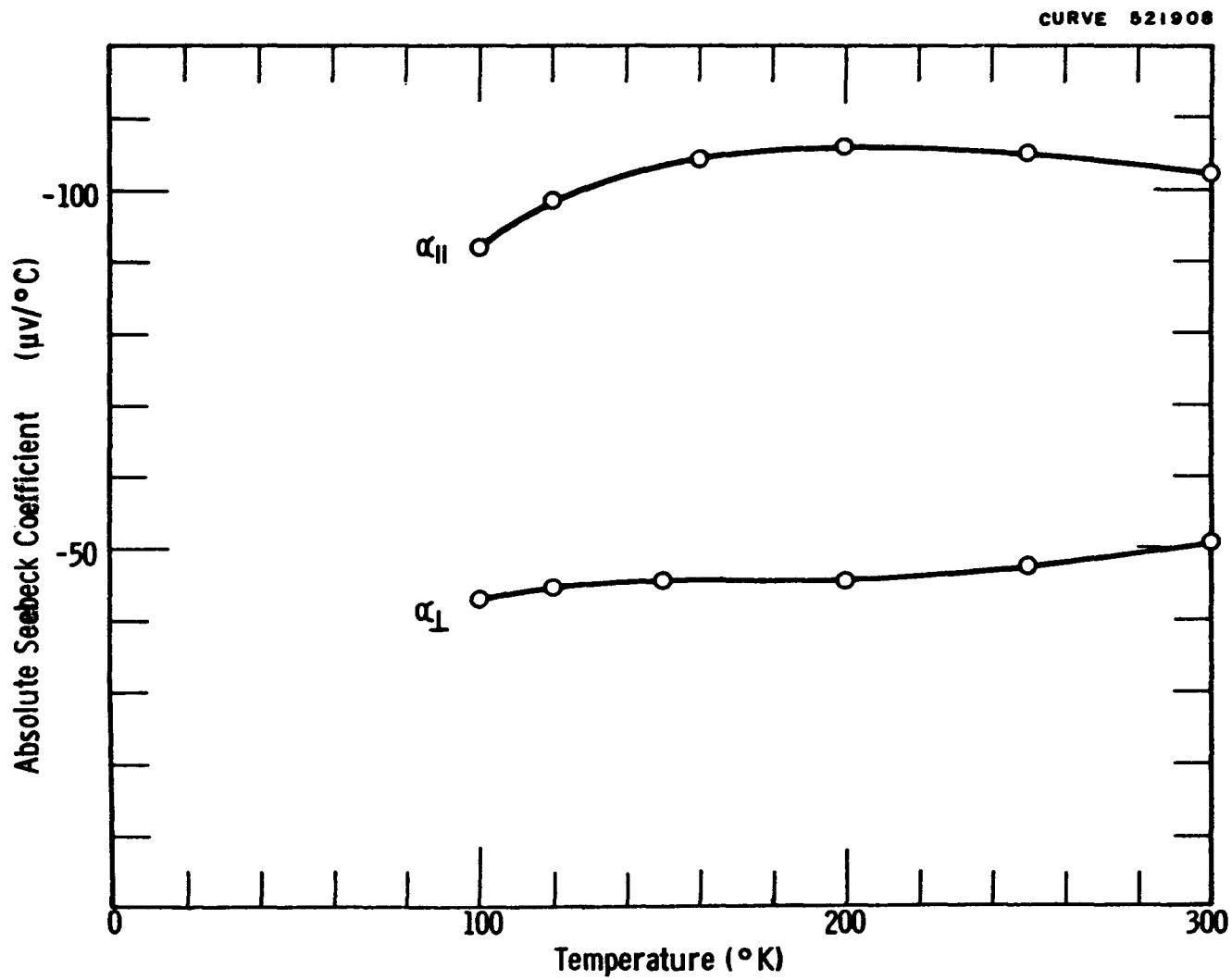

Fig. 4

Absolute Seebeck coefficient vs. temperature for pure bismuth single crystals; $\alpha_{\parallel}$ and $\alpha_{\perp}$ were calculated by fitting Eq. 2 to the data.

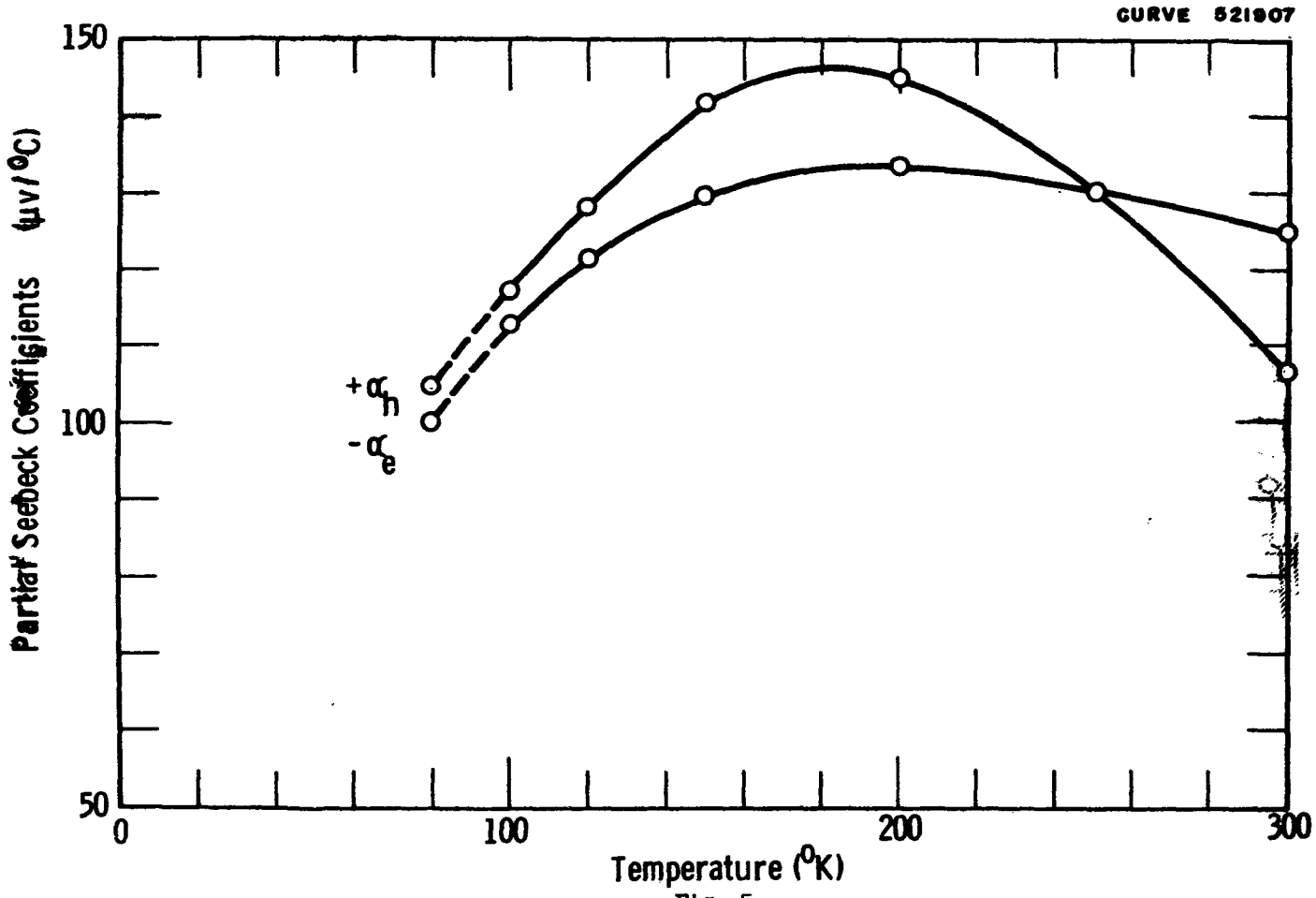

Fig. 5

The isotropic partial Seebeck coefficient of the electrons (α_e) and of the holes (α_h) vs. temperature for pure bismuth single crystals. The dotted lines are extrapolated to zero at 0°K.

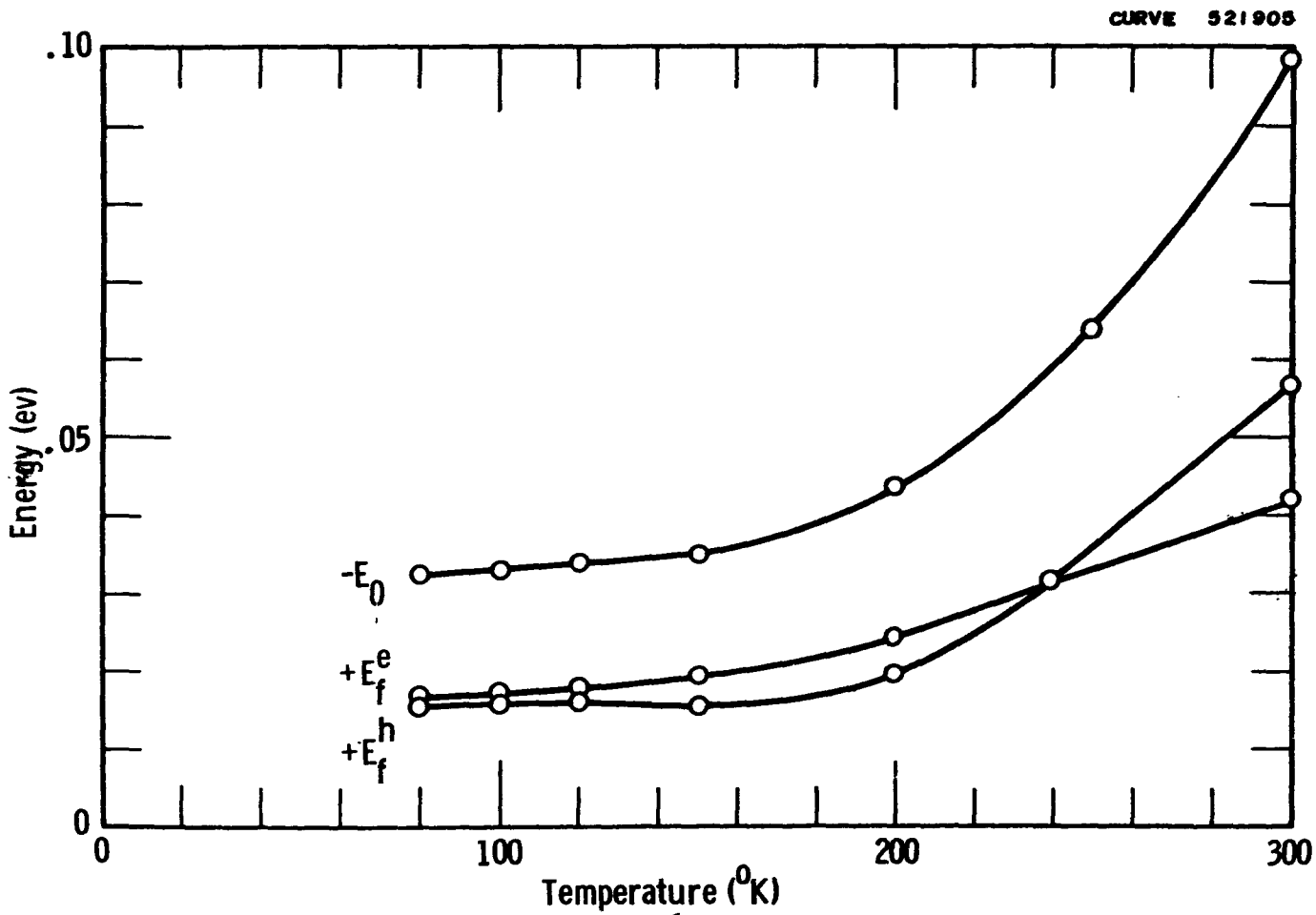

Fig. 6

The overlap energy (E_o) and the Fermi energy of the electrons (E_f^e) and holes (E_f^h) vs. temperature for pure bismuth single crystals.

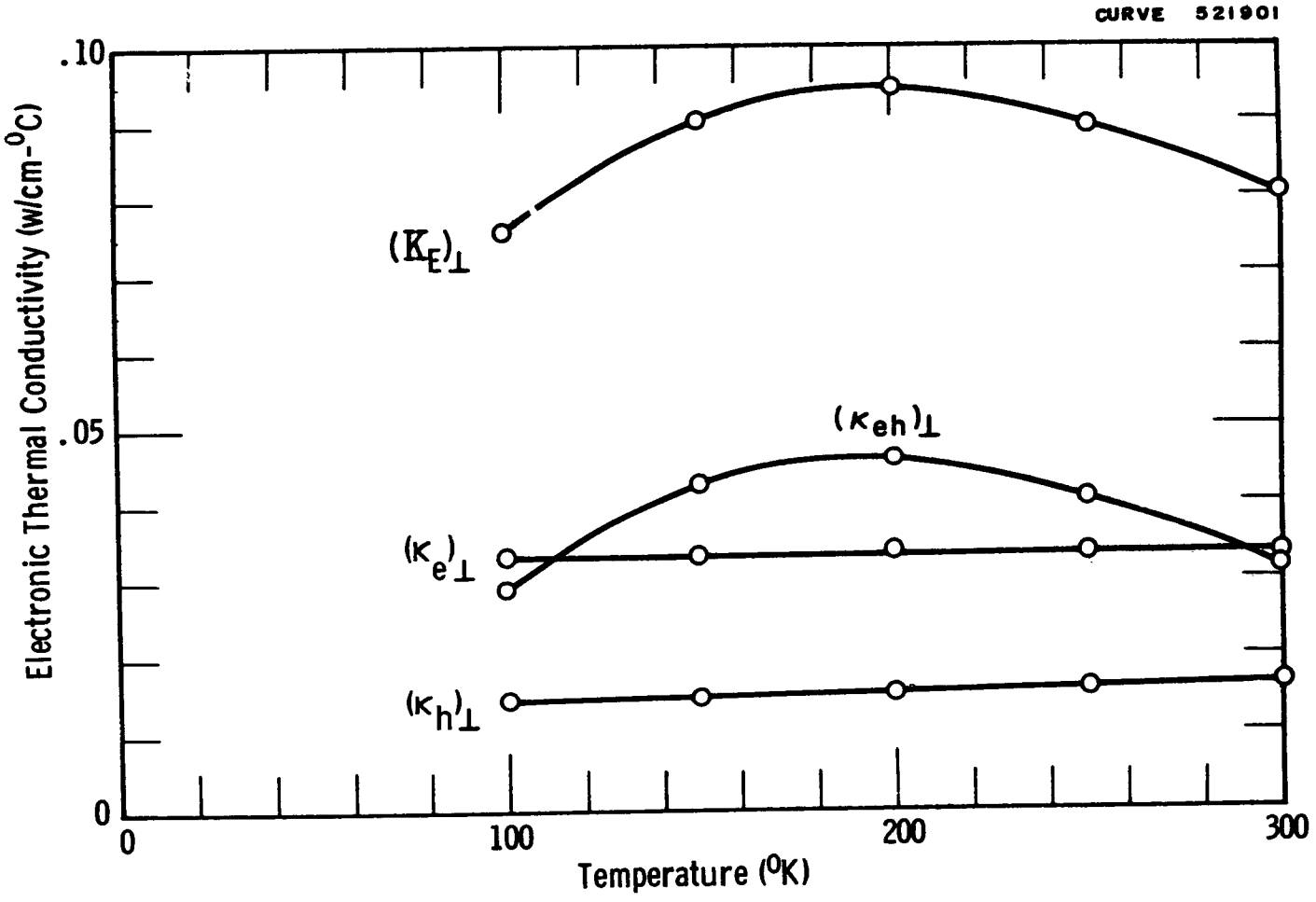

Fig. 7

The individual contributions to the total electronic thermal conductivity (K_E) for pure bismuth single crystals perpendicular to the trigonal axis. The ordinary thermal conductivity due to electrons alone (κ_e), the ordinary thermal conductivity due to holes alone (κ_h), and the thermal conductivity due to bipolar diffusion (κ_{eh}) were calculated from Eqs. 11-13. For this orientation, $(\mu_e/\mu_h)_\perp \cong 2$.

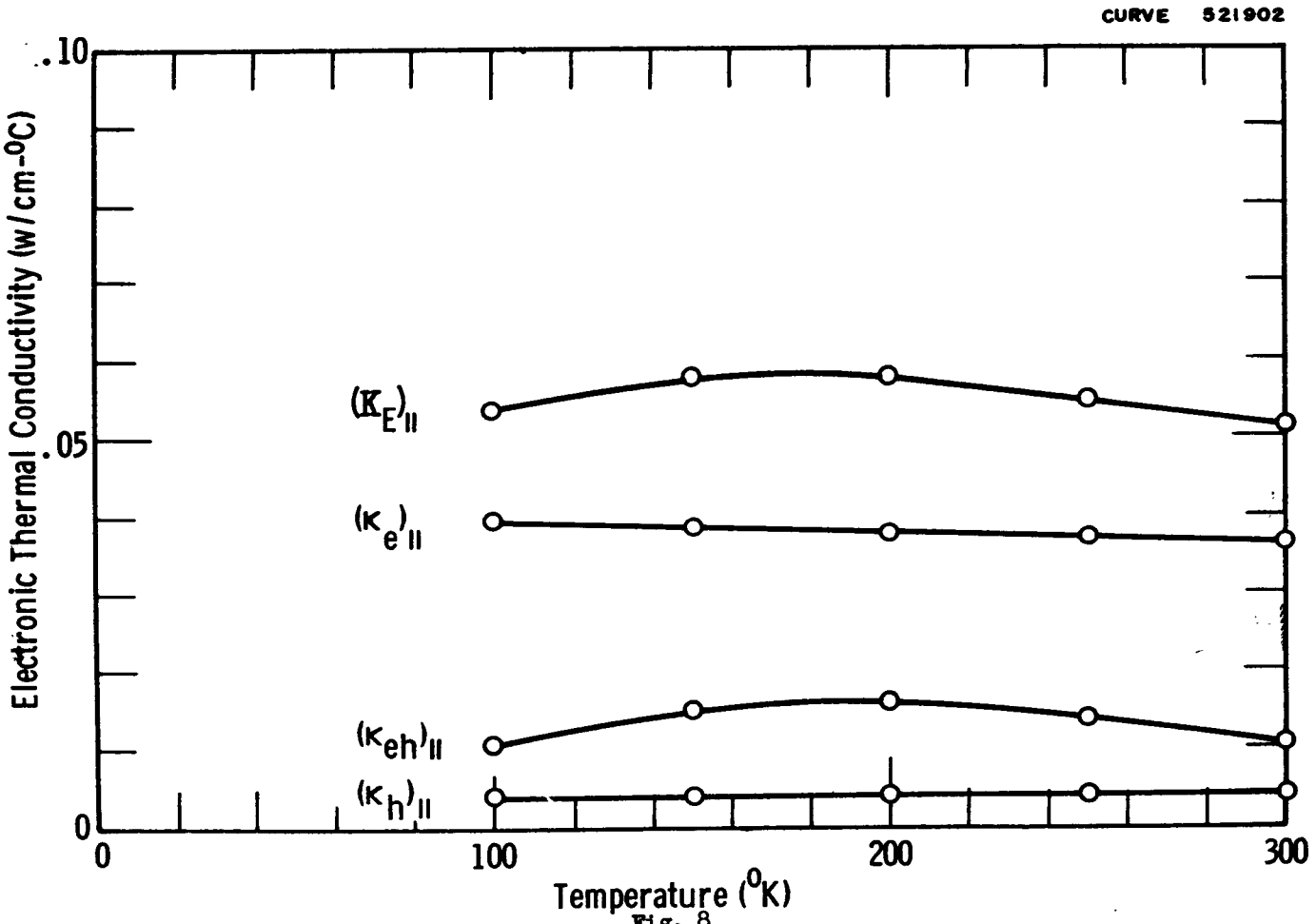

Fig. 8

The individual contributions to the total electronic thermal conductivity (K_E) for pure bismuth single crystals parallel to the trigonal axis. The ordinary thermal conductivity due to electrons alone (κ_e), the ordinary thermal conductivity due to holes alone (κ_h), and the thermal conductivity due to bipolar diffusion (κ_{eh}) were calculated from Eqs. 11-13. For this orientation, $(\mu_e/\mu_h)_{||} \cong 10$.

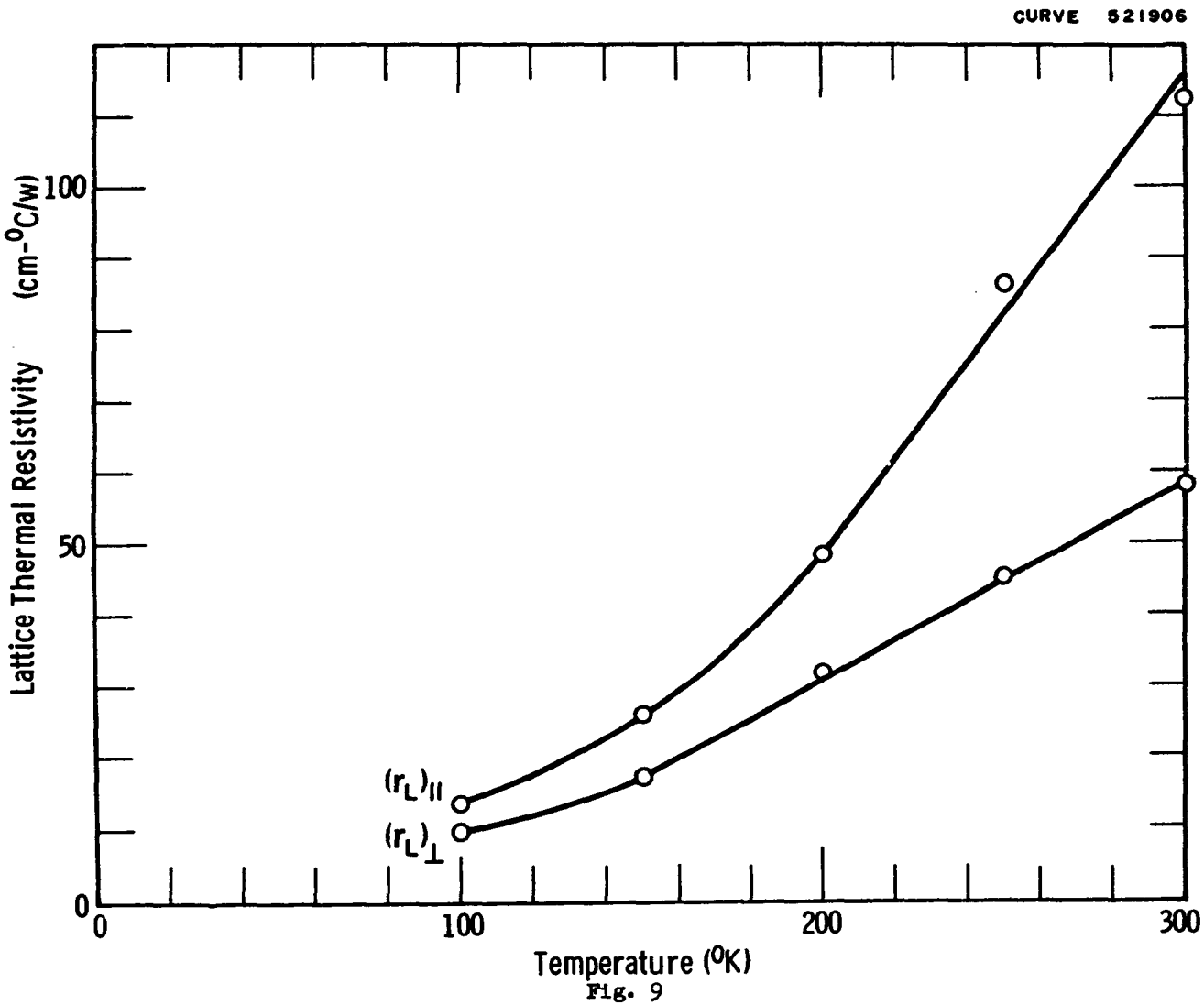

Fig. 9

The calculated lattice thermal resistivity vs. temperature for pure bismuth single crystals. The scatter at the higher temperatures is due to the fact that the lattice thermal conductivity is the difference between two large numbers in Eq. 10 as can be seen in Fig. 3.

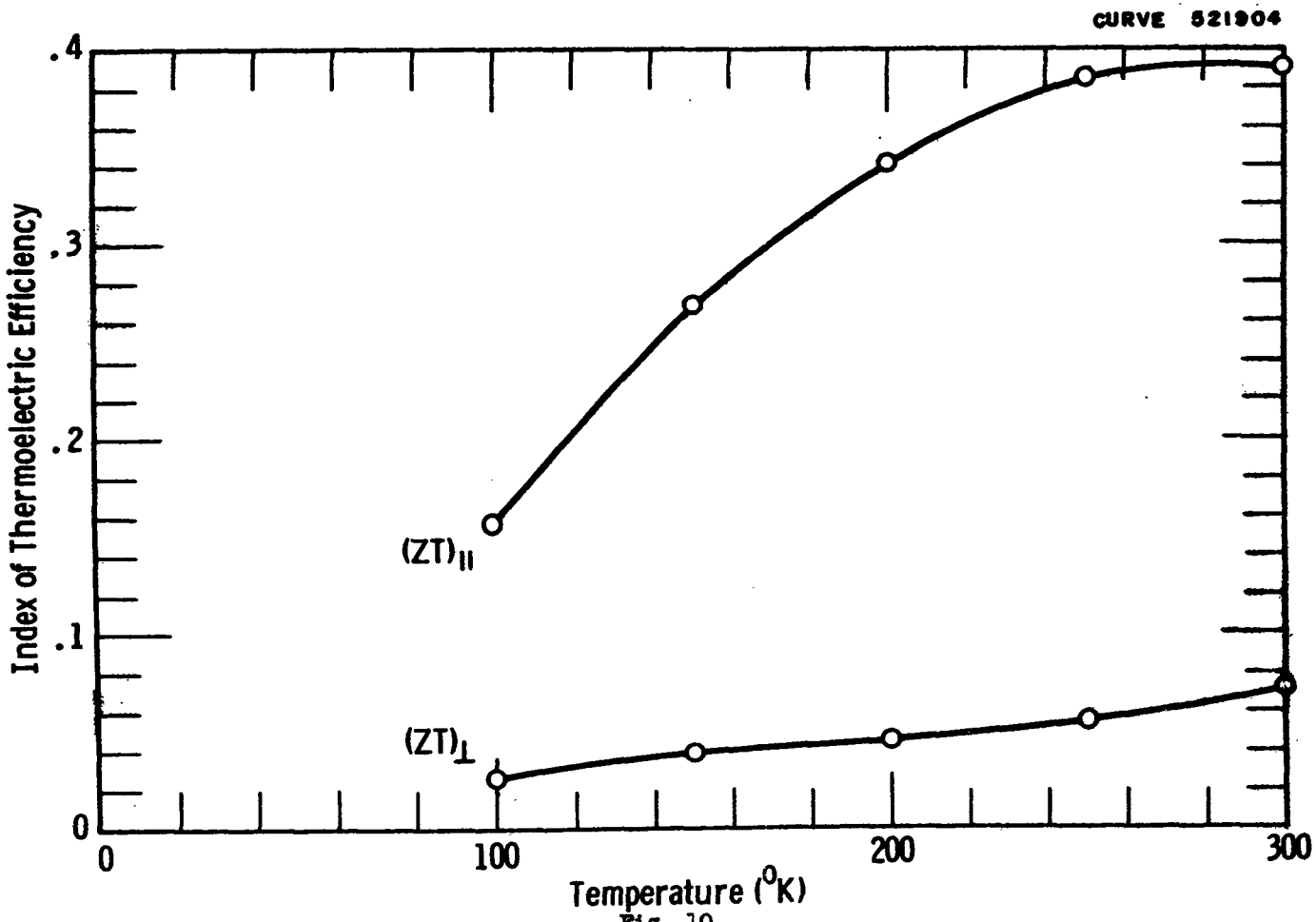

Fig. 10

The index of thermoelectric efficiency vs. temperature for pure bismuth single crystals.

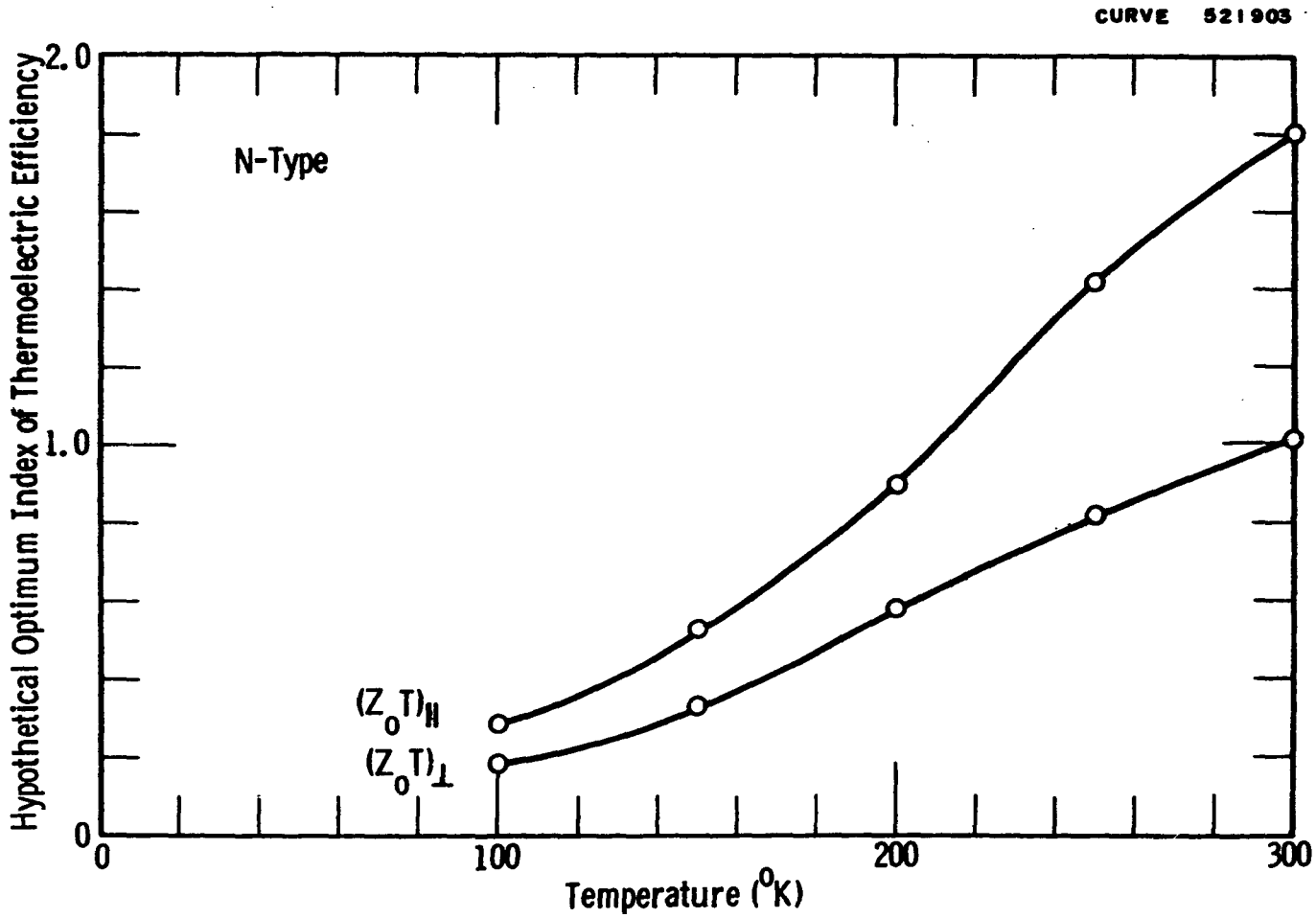

Fig. 11

The hypothetical optimum index of thermoelectric efficiency vs. temperature for "optimized N-type bismuth crystals"